

Turbulent Convection in Stellar Interiors. II. The Velocity Field

David Arnett¹, Casey Meakin^{1,2,4}, and Patrick A. Young^{1,3}

darnett@as.arizona.edu, casey.meakin@gmail.com, patrick.young.1@asu.edu

ABSTRACT

We analyze stellar convection with the aid of 3D hydrodynamic simulations, introducing the turbulent cascade into our theoretical analysis. We devise closures of the Reynolds-decomposed mean field equations by simple physical modeling of the simulations (we relate temperature and density fluctuations via coefficients); the procedure (CABS, Convection Algorithm Based on Simulations) is terrestrially testable and is amenable to systematic improvement. We develop a turbulent kinetic energy equation which contains both nonlocal and time dependent terms, and is appropriate if the convective transit time is shorter than the evolutionary time scale. The interpretation of mixing-length theory (MLT) as generally used in astrophysics is incorrect; MLT forces the mixing length to be an imposed constant. Direct tests show that the damping associated with the flow is that suggested by Kolmogorov ($\varepsilon_K \approx \rho(u')_{rms}^3/\ell_D$, where ℓ_D is the size of the largest eddy and $(u')_{rms}$ is the local rms turbulent velocity). This eddy size is approximately the depth of the convection zone ℓ_{CZ} in our simulations, and corresponds in some respects to the mixing length of MLT. New terms involving the local heating due to turbulent dissipation should appear in the stellar evolutionary equations, and are not guaranteed to be negligible. The enthalpy flux (stellar “convective luminosity”) is directly connected to the buoyant acceleration, and hence to the scale of convective velocity. MLT tends to systematically underestimate the velocity scale, which affects estimates of chromospheric and coronal heating, mass loss, and wave generation. Quantitative comparison with a variety of 3D simulations reveals a previously unrecognized consistency. Extension of this approach to deal with rotational shear and MHD is indicated. Examples of application to stellar evolution will be presented in subsequent papers in this series.

Subject headings: stars: evolution - hydrodynamics - convection - turbulence

¹Steward Observatory, University of Arizona, 933 N. Cherry Avenue, Tucson AZ 85721

²FLASH Center, University of Chicago, Chicago, IL

³School of Earth and Space Exploration, Arizona State University, Tempe, AZ

⁴Joint Institute for Nuclear Astrophysics, University of Chicago, Chicago, IL

1. Introduction

More than fifty years ago, the version of the “mixing length theory” of convection (MLT) which became the preferred basis for subsequent study of stellar evolution was introduced (Biermann 1951; Vitense 1953; Böhm-Vitense 1958). Despite much effort (still ongoing), MLT is still the standard choice for the field.

In this paper we develop a new procedure, “Convective Algorithms Based on Simulations” (CABS), in which we close the Reynolds-decomposed, angular and time averaged equations by simple physical models based upon analysis of fully three-dimensional, time dependent turbulent stellar convection (Meakin & Arnett 2007b). These simulations include convective boundaries within the computational volume (as far from the edges of the grid as feasible), and allow interface physics to be examined. The resulting theoretical formalism allows us to incorporate content from other simulations (especially Chan & Sofia (1989, 1996); Kim et al. (1995, 1996); Porter & Woodward (2000); Porter, Woodward, & Jacobs (2000); Robinson et al. (2004)), and from research in other fields, such as terrestrial fluids (Turner 1973), oceanography (Gill 1982), and meteorology (Dutton 1986), which have a firmer empirical basis. We develop a simple description of the convective velocity field as seen in our simulations. This effort brings some startling suggestions for revision of our interpretation of MLT, and suggests how our approach may be generalized to include rotation and magnetic fields (Balbus & Hawley 1998; Pessah, Chan, & Psaltis 2006). This is timely, considering recent success in simulating turbulent plasma with magnetic fields (Browning 2008; Schüssler & Völger 2008).

Since the formulation of MLT, there has been a considerable development in understanding the nature of chaotic behavior in nonlinear systems; see Cvitanović (1989) for a review and reprints of original papers, and Frisch (1995); Gleick (1987); Thompson & Steward (1986). Lorenz (1963) presented a solution to the Rayleigh problem of thermal convection (Chandrasekhar 1961) which captured the seed of chaos in the Lorenz attractor, and contains a representation of the fluctuating aspect of turbulence not present in MLT. Kolmogorov (1962) and Obukhov (1962) developed the modern version of the turbulent cascade. Although already formulated, the original theory (Kolmogorov 1941) was not used in MLT.

We derive our approximate theory from a consideration of the full equations of 3D compressible hydrodynamics for a multiple component fluid. These are close to the corresponding equations for a high beta (matter dominated) plasma. This approach will allow us to incorporate a variety of phenomena in a coherent way, and to evaluate their relative importance, rather than to patch together various bits of physics piecemeal. Here we focus on the dominant features of non-rotating, non-magnetic, turbulent, compressible fluid flow. The results are applicable to almost all stages of stellar evolution (any stage having convection or shear)¹.

¹The shear from convection is similar to the shear from differential rotation; fluid experiments may use either to investigate the physics of shear (Turner 1973). Although different in some details, there are deep connections between

In Section 2 we examine the physical aspects of stellar convection, and show that the velocity scale is set by the balance between buoyant driving, and damping in the Kolmogorov cascade. Appropriate averaging allows us to deal with mild time dependence and reveals a robust underlying behavior. We develop a kinetic energy equation describing the average properties of turbulent convection, which shows how turbulent motion is created, transported, and destroyed. In Section 3 we incorporate this theoretical development into the equations of stellar evolution with turbulent convection, including new terms. Section 4 uses the theoretical development to compare our simulations to others, and finds previously unrecognized similarities. Section 5 indicates some important implications of this work, including how the effects of burning, rotation and magnetic fields may be included. Section 6 summarizes our results and conclusions. Quantitative treatment of the dynamics of fluctuations and a comprehensive algorithm for stellar evolutionary calculations will be developed in subsequent papers in this series.

2. Physical Aspects of Stellar Convection

Stellar convection has high Reynolds numbers because of the large linear scales, and is therefore highly turbulent. Our simulations have adequate resolution to show this type of behavior. Turbulent convection has several key features that need to be modeled: (1) it is nonlocal, (2) it has strong fluctuations in both space and time, (3) it is damped by a cascade of unstable vortices down to scales small enough for microscopic processes to dissipate effectively, (4) mixing of passive scalar properties is efficient, (5) turbulent behavior spreads to fill the volume allowed, and (6) buoyant acceleration is closely related to convective (enthalpy) flux, so that convective kinetic energy is closely tied to convective luminosity. MLT incorporates (4) and imperfectly deals with (6); we will address all six issues.

Cattaneo, et al. (1991) found that 3D simulations of turbulent convection had two aspects: (1) vigorous, large scale downflows², and (2) disorganized weaker motions. These two aspects have been confirmed by many other simulations, including our own. MLT attempts to describe the average properties of the disordered aspect. We will construct a theory which includes both; buoyant acceleration is characteristic of the largest scales, and turbulent dissipation of the smallest.

2.1. The Kinetic Energy Equation

We start with the equations we used in our 3D simulations (Meakin & Arnett 2007b). We use Reynolds decomposition of relevant flow and thermodynamic variables, which separates the fluctuating from the slowly varying components (Tennekes & Lumley 1972). Numerical simula-

convective mixing as described here and the rotational mixing investigated by Meynet & Maeder (2000).

²Porter & Woodward (2000) suggest that large scale flows do dominate the energy flux.

tions dissipate features with wavelengths at or below the grid scale, and we will identify this with dissipation in the turbulent cascade (Kolmogorov 1941, 1962).

In the process of approximation of partial differential equations by finite methods, there is inevitably a loss of information at scales smaller than the grid size. A single volume element in space is approximated as a homogeneous entity; this is equivalent to complete mixing at this scale, at each time step, of mass, momentum, and energy. The loss of information that occurs with this mixing corresponds to an increase in entropy (Shannon 1948); the mixing of momentum is equivalent to the action of viscosity (Landau & Lifshitz 1959). In 3D flow, turbulent energy will cascade from large scales to small, at a rate set by the largest scales. We use an implicit sub-grid dissipation in our large eddy simulation (ILES), which is the most computationally efficient way to deal with turbulent systems with a large range of scales (Boris 2007; Woodward 2007); the largest scales, which set the rate of cascade and contain most of the energy, are resolved on our grid and explicitly calculated, while the sub-grid scales are dissipated in a way consistent with the Kolmogorov cascade.

Sytine, et al. (2000) demonstrated that PPM, the piece-wise parabolic method based on the Euler equation (which has no explicit viscosity), converges to the same limit as methods based on compressible viscous equations (which do have explicit viscosity), as the grid is refined to smaller zones and smaller effective viscosity (the relevant limit for astrophysics). Porter et al. (1999) show the compatibility of mildly compressible flow with the Kolmogorov (1941) spectrum; Kritsuk, et al. (2007) have pushed this to highly compressible flows as well. To represent the sub-grid dissipation, which is inherent in our simulations, we explicitly introduce a volumetric dissipation rate for kinetic energy, ε_K , in our theoretical analysis. However, the turbulent cascade is a property of the whole convective flow, so connection to turbulence theory must be made through *integrals* of ε_K over the convection zone. Note that this is different from defining ε_K as a function of *local* variables (e.g., Smagorinsky (1963); Chan & Sofia (1989); Hansen & Kawaler (1994); Asida & Arnett (2000)); see below.

The kinetic energy (KE) equation for convective motion was given in Meakin & Arnett (2007b). Taking the scalar product of the velocity with the equation of motion, we decompose the convective velocity \mathbf{u} , the density ρ , and the pressure p into mean and fluctuating components (e.g., $p = p_0 + p'$, so the time averages are $\bar{p} = p_0$ and $\bar{p}' = 0$). This choice of just \mathbf{u} , p , and ρ for this Reynolds decomposition into average and fluctuating parts gives the simplest equation for kinetic energy; the velocity \mathbf{u} is derived from buoyancy and pressure forces (ρ and p fluctuations).

Using the hydrostatic equilibrium condition, and performing averages, gives (see eq. A.12 in Meakin & Arnett (2007b)),

$$\begin{aligned} \partial_t \langle \overline{\rho E_K} \rangle + \nabla \cdot \langle \overline{\rho E_K \mathbf{u}_0} \rangle = \\ - \nabla \cdot \langle \overline{\mathbf{F}_p + \mathbf{F}_K} \rangle + \langle \overline{p' \nabla \cdot \mathbf{u}'} \rangle \\ + \langle \overline{\rho' \mathbf{g} \cdot \mathbf{u}'} \rangle - \varepsilon_K. \end{aligned} \tag{1}$$

We use $\langle p \rangle$ to denote an average over angles at constant radius. The time average is taken over durations greater than a transit time $t_{transit} = \ell_{CZ}/(u')_{rms}$, where ℓ_{CZ} is the depth of the convective region, and $(u')_{rms}$ is the rms velocity across this region. This smooths the fluctuations, gives a nonlocal character to the analysis, and implies a separation of time scales into short ($t \ll t_{transit}$) and long ($t \gg t_{transit}$). We consider the case in which we may integrate over these short time scales and explicitly calculate the evolution on the long time scales.

Here E_K is the kinetic energy per unit mass, ρ the mass density, \mathbf{u}_0 is the nonfluctuating part of the fluid velocity vector and \mathbf{u}' its fluctuating part, so

$$\mathbf{F}_p = p' \mathbf{u}' \quad (2)$$

is the energy flux due to pressure perturbations carried by fluctuations (this pressure-velocity correlation flux reduces to the acoustic flux when considering sound waves, Landau & Lifshitz (1959), p. 251, and contains the energy flux due to internal gravity waves),

$$\mathbf{F}_K = \rho E_K \mathbf{u}' \quad (3)$$

is the flux of kinetic energy carried by convective turbulent motion, \mathbf{g} is the gravitational acceleration vector, and ε_K is the volumetric rate of dissipation implied by the turbulent cascade down to small scales.

2.2. Boundaries

The location of convective boundaries is a long-standing problem in stellar astrophysics. It has long been known that some sort of "convective overshooting" is necessary for models to match observations. This has been conceived as mixing of material beyond the convective boundary, often by "penetrative convection". This problem exists in part because the convective boundary has been inappropriately defined (Meakin & Arnett (2007b), especially §4.1 and §7). The standard definition used in mixing length theory defines the convective boundaries using the thermodynamic nablas, which essentially mark the onset and cessation of buoyant acceleration. One of the essential properties of convection is that turbulence fills the space available. A more appropriate criterion is one in which the stellar background is stiff enough to contain the turbulent convection, and therefore must account for the relative strength of the turbulent flow and the elastic stable layers.

We will define the convective zone as that region in which the stratification of the medium is unstable to turbulent mixing. This is evaluated with the "bulk Richardson number"

$$Ri_B = \Delta b l / u^2, \quad (4)$$

where $\Delta b = \int_{\Delta r} N^2 dr$ is the buoyancy jump across a layer of thickness Δr in the radial direction, N^2 is the Brünt-Väisälä frequency, u is the rms velocity providing shear, and l is the scale length of the turbulence (essentially the size of the largest eddies). The precise definition of the thickness

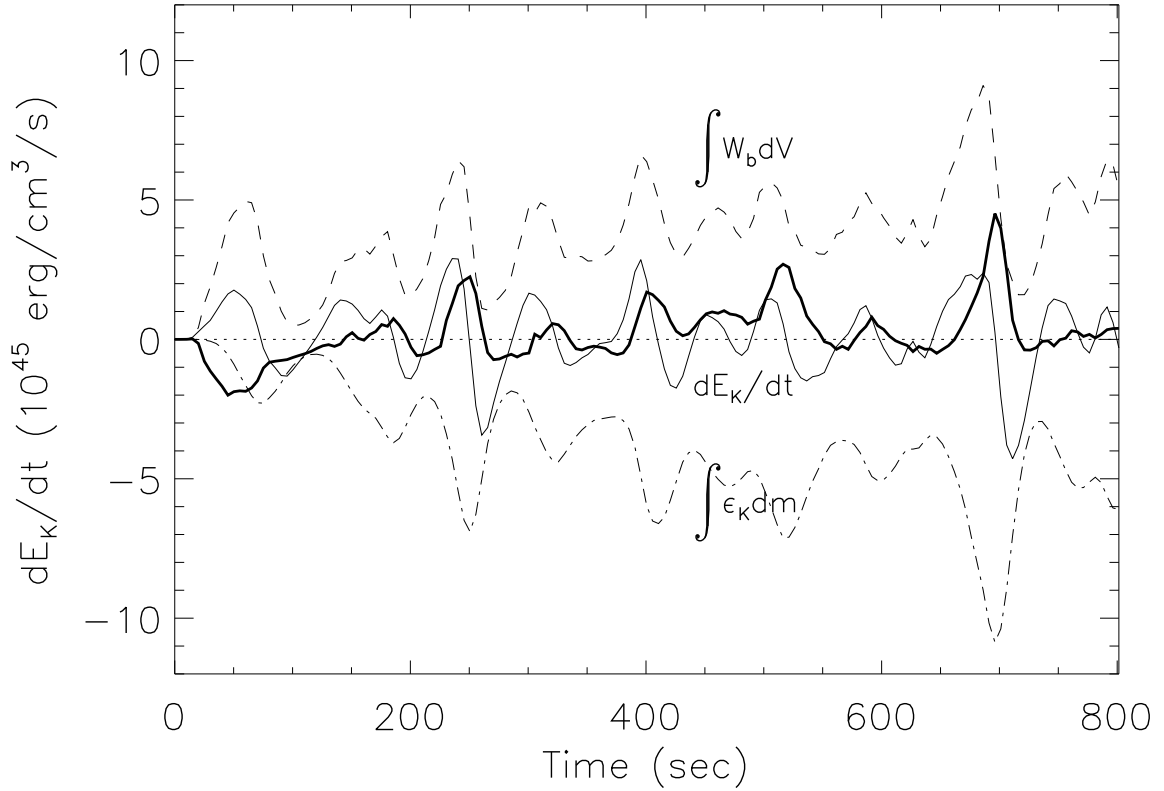


Fig. 1.— Behavior of global quantities in the convection zone, which affect the turbulent kinetic energy, entrainment, and gravity wave generation at the convective boundaries. The thick line is the sum of all terms except entrainment and boundary wave luminosity, and indicates when entrainment events are vigorous (Meakin & Arnett (2007b), Fig. 4). The buoyancy driving $B = \int W_b dV$ is compensated for by the turbulent damping $D = \int \epsilon_K dV$. The time derivative of the kinetic energy in the convection zone is denoted $dE_K/dt = \frac{d}{dt} \int \rho (u')_{rms}^2 dV$. There is a slow increase in amplitude due to lack of balance between nuclear heating and neutrino cooling (see Fig. 5 below and Arnett (1996)).

Δr is a topic deserving further study; in several cases we have noticed that the rapid change in N^2 near a boundary tends to make Δb insensitive to the exact value of Δr chosen for integration to obtain Δb .

In the linear limit of plane parallel flow, a region with $Ri_g \lesssim 0.25$ has enough kinetic energy to overcome the stable stratification (Dutton 1986). Here Ri_g is the “gradient” Richardson number, and is a locally defined quantity, used in a linear stability analysis. The “bulk” Richardson number Ri_B is an inherently nonlinear quantity based on integration over an extended region. Since $Ri_{g,crit} > 0$, this allows for $N^2 > 0$ as well. This formulation recognizes that layers that are thermodynamically stable (real roots to N^2) can be hydrodynamically unstable when kinetic energy is input to the zone. The bulk Richardson criterion allows more mixing than predicted by the Ledoux criterion; the Schwarzschild criterion ignores compositional effects, and also predicts more mixing than Ledoux (see Kippenhahn & Weigert (1990); Hansen & Kawaler (1994)).

Stable regions adjacent to the convective zone will become Richardson unstable periodically as shear builds up from adjacent turbulent motions and waves generated by convection, leading to entrainment of material at convective boundaries (Fernando 1991). The bulk Richardson number is not only an indicator of a convective boundary; it also determines the “rate” at which the boundary migrates through the lagrangian mesh by mixing processes (Meakin & Arnett 2007b), and thus provides a “dynamic” boundary condition for the flow.

2.3. Averages

Our analysis is based primarily upon the numerical simulations of oxygen shell burning in a $23M_\odot$ star, but is found to be broadly applicable to other examples of stellar convection (such as convective envelopes, which are driven by the superadiabatic layer at the top rather than the nuclear burning shell at the bottom). Our convective zone has a depth of two pressure scale heights (see Meakin & Arnett (2007b) for detail).

Why do we need to do averaging? Fig. 1 shows the behavior of the largest terms in the kinetic energy equation (averaged over the convection zone), throughout the duration of the simulation. The dominant terms are the integrals of the buoyancy driving $\int W_b d\mathcal{V} = \int g\rho'u'd\mathcal{V}$, which is positive, and of damping, $\int \varepsilon_K d\mathcal{V}$, which is negative. Both show recurrent bursts (ten in 800 seconds). The time derivative of kinetic energy in the convection zone (labeled dE_K/dt) is constant on average. The remaining bumps are due to missing terms (divergence of F_P and F_K).

We saved complete data every 0.5 seconds, which was adequate for making movies, and constructing averages of motion. A key issue is distinguishing between turbulent velocities and wave velocities with such a coarse stride in time. We have found a way to split the velocity averages into turbulent and wave components for better accuracy in the analysis (see Appendix A for a detailed discussion of how this is done).

Table 1. Kinetic Energy Equation Terms Averaged over Convection Zone and over four transit times (erg/s)

| Term | Value | Term | Value |
|--|------------|--|------------|
| $\int \langle \overline{W_B} \rangle d\mathcal{V}$ | 4.576(45) | $-\int \langle \overline{\varepsilon_K} \rangle d\mathcal{V}$ | -4.677(45) |
| $-\int \langle \overline{\nabla \cdot F_K} \rangle d\mathcal{V}$ | 2.584(44) | $-\int \langle \overline{\nabla \cdot F_P} \rangle d\mathcal{V}$ | -9.922(43) |
| $-\int \langle \overline{dE_K/dt} \rangle d\mathcal{V}$ | -5.790(43) | $\int \langle \overline{p' \nabla u'} \rangle d\mathcal{V}$ | -1.516(41) |

The level of complexity shown in Fig. 1 is daunting, but the near balance of buoyant driving and turbulent damping provides a clue.

The system is simplified if we integrate over time; the resulting values over four transit times are shown in Table 1. We do not calculate the damping directly, but deduce it as the remainder left from the other five terms, so that the entries sum to zero. We are comfortable with this procedure because of the good conservation properties of the numerical simulations.

The dominance of buoyant driving and damping is now clear; the next largest term is the divergence of the kinetic energy flux, at less than 6 percent of the buoyancy term.

Suppose the globally-averaged damping term has the Kolmogorov form, so that

$$\int_{CZ} \varepsilon_K d\mathcal{V} = M_{CZ} v_{rms}^3 / \ell_D, \quad (5)$$

where ℓ_D is a constant "damping length," and v_{rms} is the rms velocity determined over the entire convection zone. For a turbulent spectrum, ℓ_D is taken to be the largest length scale (Landau & Lifshitz 1959). In what follows we will use the term Kolmogorov damping to mean damping due to a turbulent cascade to small scales, having this cubic dependence on rms velocity.

Unlike MLT, we relate the damping length to the *largest* scale in the flow; this may be thought of as a "coherent structure" or a "plume which traverses the depth of the convection zone." It is not a free parameter. We introduce the notation

$$\alpha_D = \ell_D / \ell_{CZ}, \quad (6)$$

so that α_D would be constant if the size of the largest eddy scales simply with the depth of the convection zone. Kritsuk, et al. (2007) found the Kolmogorov damping to be very close to constant during a statistical steady state in their 3D (2048^3) simulations.

Table 2. Time Scales

| Time scale | Definition | Value(seconds) |
|------------------|------------------------|----------------|
| Buoyant rise | $\int W_b dV / KE$ | 14.1 |
| Velocity damping | ℓ_D / v_{rms} | 27.6 |
| KE damping | $\ell_D / (2v_{rms})$ | 13.8 |
| Transit time | ℓ_{CZ} / v_{rms} | 51.4 |
| Turnover time | $2\ell_{CZ} / v_{rms}$ | 102.8 |

The mass contained in the convection zone is $M_{CZ} = 1.84 \times 10^{33}$ g and the total kinetic energy is $\int E_K dV = 8.61 \times 10^{46}$ ergs so that the rms velocity is $v_{rms} = 9.66 \times 10^6$ cm/s. This gives $\ell_D = 3.56 \times 10^8$ cm $\approx 0.85 \ell_{CZ}$. It is natural to compare the damping length to the depth of the convection zone. Not only is ℓ_{CZ} the largest length available for an eddy, but if measured in pressure scale height units (ℓ_{CZ}/H_P), it indicates the degree of thermodynamic anisotropy across the convective region.

Table 2 gives several relevant time scales in seconds. Although these times are short in human terms, they are much closer to thermal relaxation times than are the corresponding numbers for deep simulations of the solar convection zone (our simulations are much more relaxed in this sense).

We may write the global damping as $M_{cz} v_{rms}^3 / \ell_D = \frac{1}{2} M_{cz} v_{rms}^2 / (\ell_D / 2 v_{rms})$, and see that the damping time for kinetic energy in the convective zone is half the time to transit a damping length (which is approximately the depth of the convection zone). The *turnover* time for the convection zone is 2τ , where $\tau = \ell_{CZ} / v_{rms}$ is the transit time, to be precise. The rise time for kinetic energy and the corresponding damping time are similar (14 seconds), and much shorter than a turnover time.

The term “convective efficiency” in the stellar context is usually taken to mean that the time scale for convective energy transport is much less than the time scale for radiative energy transport (Hansen & Kawaler (1994), p. 187); this insures that the actual temperature gradient is only slightly in excess of the adiabatic one. Convection can also be thought of as a thermodynamic cycle, taking a time $2\ell_{CZ} / v_{rms}$. As we saw above, the dissipation time scale for kinetic energy is about one-seventh of this (0.134), so that in this sense, convection is not thermodynamically efficient at all, but requires continual work to keep it running. The two uses of “efficiency” causes confusion, and downplays the fact that stellar convection is *highly* dissipative, even for slightly superadiabatic temperature gradients.

2.4. Anisotropy and Kinetic Energy

Here we present an initial, qualitative discussion of the structure of the flow, which we are investigating quantitatively for subsequent publication. We extend the idea of Cattaneo, et al. (1991) that the convective velocity field has two components, a more ordered global flow and a chaotic turbulent flow. We focus on the source and sink for convective kinetic energy. Gravitational acceleration breaks the symmetry of space; we choose our z -axis parallel to this acceleration. Buoyant acceleration starts an anisotropic flow in the z direction. The flow is unstable, and begins to break up into smaller scales, and becoming more isotropic.

Suppose that the flow occurs in narrow, vigorous down plumes and slow wide upflows for convective zones with significant anisotropy. The kinetic energy in such a downflow would dominate that in the upflow; the kinetic energy flux has two more powers of velocity than the mass flux, so

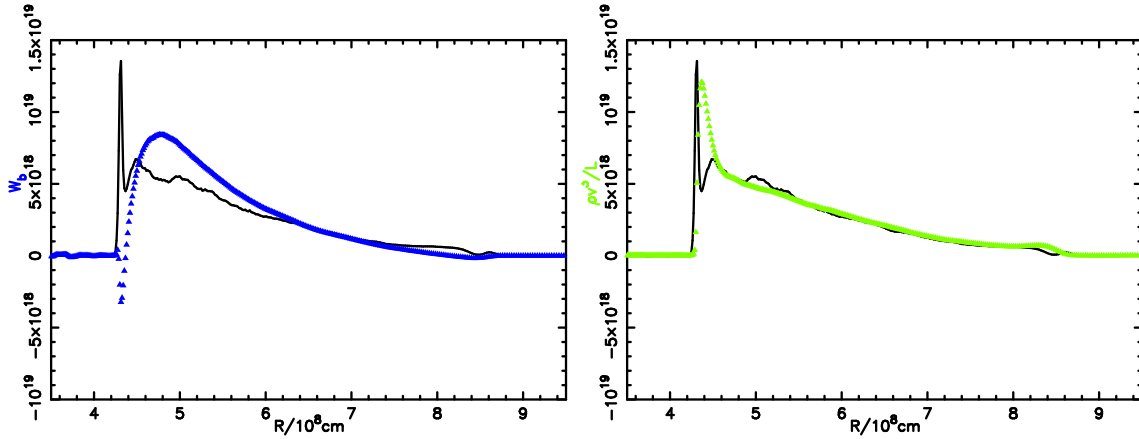


Fig. 2.— Comparison of terms in the kinetic energy equation, averaged over four transit times and over angle, as a function of radius. The solid line is the inferred local value of the volumetric dissipation due to the turbulent cascade. The thick line of triangles represents a term in the equation for kinetic energy density (Eq. 1). Buoyancy driving (left) and ε_K approximated as $\rho u_{rms}^3 / \ell_D = 1.54 \rho u_t^3 / \ell_D$ (right) are shown. Here we distinguish between the global rms convective velocity v_{rms} and the rms convective velocity at a given radius, $\langle u'^2 \rangle^{1/2} = (u')_{rms}$. We find $\varepsilon_K = (v_{rms})^3 / \ell_D$ for $\ell_D = 3.5 \times 10^8 \text{ cm} \approx \ell_{CZ}$, *globally*, and with this choice of damping length, the *local* damping per unit mass is proportional to u_{rms}^3 / ℓ_D . Much of the variation shown in the bottom panel is simply due to the density gradient (see the angular velocities in Meakin & Arnett (2007b), Fig. 6, left panel, and the background density structure in their Fig. 2, top left panel). Note that, as shown, the signs of the terms are consistent with the kinetic energy equation, so that up means increasing, down decreasing kinetic energy for the terms indicated by triangles.

that the fastest flows dominate the kinetic energy budget (Meakin & Arnett 2007b). We separate the kinetic energy into two components, $u_a^2/2$, which corresponds to the largest eddies and $u_b^2/2$, which represents all of the turbulent cascade. The turbulent instability begins to make the flow more isotropic, so that

$$u_z^2 \approx u_a^2 + u_b^2, \quad (7)$$

in the z -direction (see Ch. VI in Batchelor (1960)). If this kinetic energy is shared with the two perpendicular directions, then

$$u_x^2 + u_y^2 \approx u_z^2. \quad (8)$$

Further, it seems that the cascade component in the z -direction is similar to the components in the x - or the y -directions, $u_x^2 \approx u_y^2 \approx u_b^2$. While the downflow matter is balanced by a return flow in x and y , the return flow is slower and broader (by our assumptions), with lower kinetic energy (which we neglect here). Thus

$$u_b^2 \approx u_a^2. \quad (9)$$

One quarter of the kinetic energy is in the largest scale component $u_a^2/2$. The ratio of vertical to horizontal rms velocities is therefore $u_x/u_z \approx 1/\sqrt{2}$.

How does this simple model compare with simulations? In Fig. 6, Meakin & Arnett (2007b) give the rms values of velocity in the vertical (v_r) and the horizontal (v_θ and v_ϕ) directions. We identify locally the r direction with the z -axis, and theta and phi with the x and the y axes. Then from their Figure 6, we find

$$0.5 \leq u_x/u_z \approx u_y/u_z \leq 0.8, \quad (10)$$

over the convection zone, away from the boundaries. The measured value of the vertical velocity contains both large scale and cascade components. This is consistent with our estimate of $u_x/u_z \approx u_y/u_z \approx 1/\sqrt{2} \approx 0.707$. The large scale component of kinetic energy is comparable to the cascade one, consistent with Cattaneo, et al. (1991), and our simulations.

The simulations have led us to a simple, two-component model for the origin and destruction of convective kinetic energy. Anisotropy is due to buoyant acceleration in the largest eddy, which represents one component. The second is isotropic turbulence, which gives dissipation of kinetic energy after the cascade to small scales. It will be interesting to test and refine this model against a wide variety of simulations. The power spectra of the flow will be a useful tool to explore this ansatz.

In what follows we will define a turbulent rms velocity u_t from the measured horizontal velocity components, $u_t^2 = \frac{3}{2}(u_x^2 + u_y^2) = \frac{3}{4}u_{rms}^2$. We note for future reference that $u_{rms}^3/u_t^3 = (\frac{4}{3})^{\frac{3}{2}} = 1.540$. Roughly speaking, we identify u_t with the turbulent cascade. The anisotropic component u_a is identified predominately with the largest turbulent scale, and may be sensitive to the structure of the convection zone and the location and strength of the buoyant acceleration.

2.5. Radial variation of Averages

We now relax one level of averaging, and consider the radial variation of all the terms in the kinetic energy equation. Figures 2, 3 and 4 show six terms in six panels, each compared to the inferred damping (the solid line present in each panel). This allows us to determine what each of five terms contribute to the inferred damping, and also shows an isotropic Kolmogorov estimate as a simple approximation (Fig. 2, right panel). The solid line has a sharp spike at the bottom of the convection zone. This feature is due to the dominance of g-mode character in the motion near the boundary region. The Kolmogorov cascade is appropriate away from the boundaries.

In Figure 2, the left panel shows the averaged buoyancy $\int \overline{\langle W_B dV \rangle}$, and the right panel shows the isotropic Kolmogorov approximation, both as dotted curves. In planar geometry (a fair approximation), we can relate this quantity to the "buoyancy flux" which is widely used in experimental fluid mechanics (Turner 1973). The buoyancy flux is

$$\mathbf{q} = \overline{\langle \mathbf{g} \cdot \mathbf{u}' \rho' \rangle} / \rho_0, \quad (11)$$

so that $\int \overline{\langle W_B dV \rangle} \rightarrow \int \overline{\langle q \rangle} 4\pi r^2 dr$. The enthalpy (convective heat) flux is

$$\mathbf{F}_e = \overline{\langle \rho_0 \mathbf{u}' C_p T' \rangle}, \quad (12)$$

where C_p is the specific heat at constant pressure. For low Mach number flows like ours³ the pressure fluctuations are small. The temperature and density perturbations at constant pressure are proportional,

$$\rho' / \rho_0 = \beta_T T' / T_0, \quad (13)$$

where $\beta_T = -\partial \ln \rho / \partial \ln T \Big|_P$, taken at constant pressure (and composition)⁴. We find, using hydrostatic equilibrium of the unperturbed star $H_p g = P_0 / \rho_0$,

$$\mathbf{F}_e = \rho_0 H_p \mathbf{q} / \nabla_a. \quad (14)$$

where $\nabla_a = \beta_T P / \rho C_p T$, a factor that we will see again. Except possibly for extreme cases, the enthalpy flux F_e , which is intimately related to the stellar luminosity, is itself closely related to the buoyancy flux q and *hence to the convective velocity* (see also Meakin & Arnett (2007b)). MLT ignores this connection; we shall exploit it. The source of turbulent kinetic energy is directly proportional to the convective luminosity and thus to the radial entropy gradient ("superadiabatic gradient") of MLT.

³As we discuss below, simulations with stiffer equations of state will have larger pressure fluctuations. We expect the neglected terms to be important for wave generation, but probably in a restricted volume of the convection zone.

⁴In Meakin & Arnett (2007b) we denoted this quantity by β_T ; the subscript T is to avoid confusion both with Eddington's use of β for the ratio of gas to total pressure, and the fluid dynamics community use of β as the adverse temperature gradient.

Buoyancy is one of the two dominant terms, and with a sign opposite to that of the damping; it differs in magnitude from the inferred damping at the convective boundaries (lower) and the broad peak above the bottom of the convection zone (higher).

The right panel shows the isotropic Kolmogorov approximation to the *local* damping, $M_{CZ} u_{rms}^3 / \ell_D = 1.54 M_{CZ} u_t^3 / \ell_D$. The condition of global balance between all driving and damping terms gives a value for ℓ_D , but the local value of u_t is used. This gives a relatively good, smoothed fit to the actual inferred damping throughout the turbulent convection zone, and departs only in the boundary layers where the velocity field is due primarily to gravity waves. *The net effect of the remaining terms in the KE equation is to modify the velocity field so that the damping is more smoothly distributed over the turbulent region than is the driving.*

The agreement in Figure 2, right panel, between the actual inferred dissipation and our estimate provides strong support for our introduction of the “Kolmogorov dissipation” in both its global and local forms.

Fig. 3 shows the spatial behavior of the flux divergence terms, $\nabla \cdot \mathbf{F}_K$ for flux of kinetic energy and $\nabla \cdot \mathbf{F}_P$ for the pressure correlation flux. These terms have significant positive and negative contributions, which cancel upon averaging over radius, and therefore are more important than Table 1 would suggest. The change of sign in a divergence implies that these terms move kinetic energy. In particular, they remove kinetic energy from the region where buoyancy is strong, and add it to regions where the buoyancy is weak. The divergence of the kinetic energy flux (Fig. 3, left panel) is the most significant in transporting energy. It moves kinetic energy from the region in which buoyancy driving exceeds the inferred damping, and toward the convective boundaries.

In Fig. 2, left panel, we saw that there is negative buoyancy at the convective boundaries; this is due to buoyancy braking of the convective motion. The pressure correlation flux (Fig. 3, right panel) is most effective in the deficit regions right at the convective boundary, and generates elastic response (waves) in the stably stratified regions outside the convection zone. This two-step behavior, with first F_{KE} and then F_P carrying energy to the edge of the convection zone, is mirrored at the upper convective boundary, but at lower amplitude.

The $p' \nabla \cdot u'$ term, shown in the left panel of Fig. 4, does the same sort of thing at a much reduced level. In the right panel is shown the time derivative of the kinetic energy, which is small. The convection is close to a steady state behavior.

There is a simple picture which explains these trends. (1) The extent of turbulence is limited by energy and by boundaries. In a star, turbulence will mix even stably stratified layers so long as sufficient kinetic energy is available to supply the work necessary. (2) Turbulence takes ordered motion on the large scales and converts it to disordered motion on small scales. It makes the flow more isotropic. Kolmogorov dissipation is derived with the assumption of homogeneity and isotropy, and so becomes a better approximation as turbulence acts.

The convective motion is driven by buoyant acceleration, parallel to the gravitational acceler-

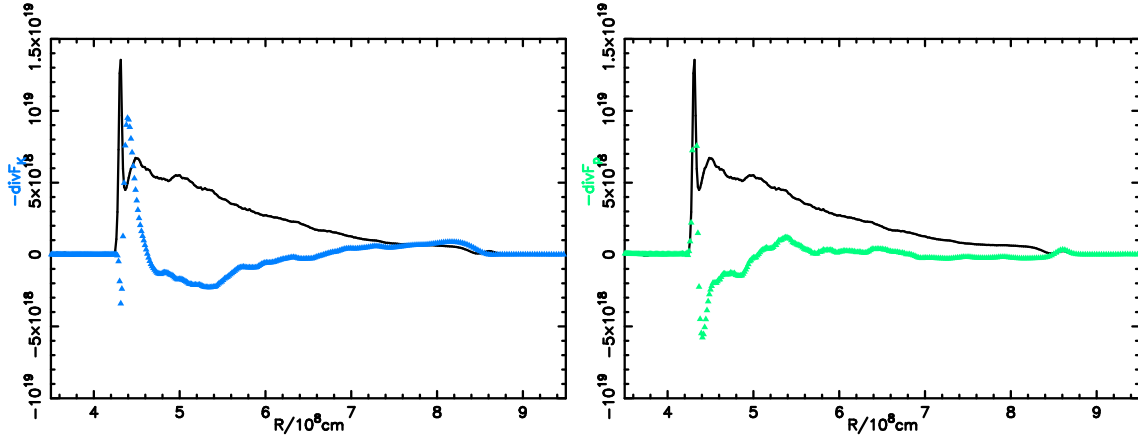


Fig. 3.— Comparison of terms in the kinetic energy equation, averaged over four transit times and over angle, as a function of radius. The solid line is the inferred local value of the volumetric dissipation due to the turbulent cascade. The thick line of triangles represents a term in the equation for kinetic energy density (Eq. 1). Divergence of F_K (left) and divergence of F_P (right) are shown. The terms for divergence of flux are important at the boundaries; they smooth the distribution of kinetic energy, causing the turbulent velocity to approach the form required for Kolmogorov damping.

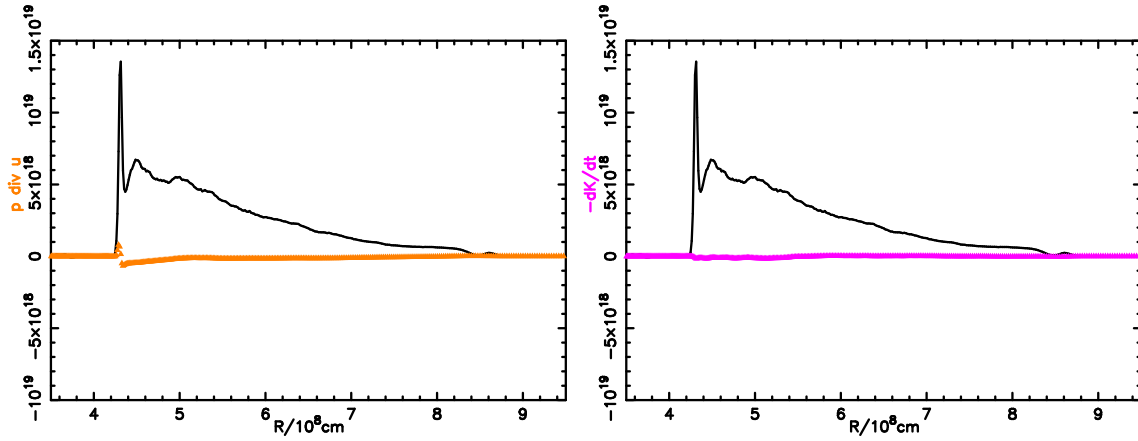


Fig. 4.— Comparison of terms in the kinetic energy equation, averaged over four transit times and over angle, as a function of radius. The solid line is the inferred local value of the volumetric dissipation due to the turbulent cascade. The thick line of triangles represents a term in the equation for kinetic energy density (Eq. 1). The terms $p'\nabla \cdot u'$ (left) and dE_K/dt (right) are shown. The effects of $p'\nabla \cdot u'$ are small and most noticeable at the lower boundary. The change in the average kinetic energy is smaller still.

ation vector, and is necessarily large-scale and anisotropic. The large-scale order of this motion is destroyed by turbulence, which spreads through all accessible regions. Thus, over all the convective region, except right at the boundaries, the flow is made more isotropic, and the Kolmogorov damping becomes better approximated by the local isotropic expression

$$\varepsilon = \rho(u')_{rms}^3/\ell_D, \quad (15)$$

(per unit volume). After carefully distinguishing between global Kolmogorov damping (Eq. 5) and the local version (Eq. 15), we find that turbulence tends to drive fluxes in such a way as to make both valid.

2.6. The Phase Shift between Damping and Driving

Having explored the spatial dependence of the KE equation, we now examine its time dependence. The flow, while wildly fluctuating, has an orderly statistical behavior. To see this, we examine the behavior of kinetic energy, integrated over the volume of the convection zone, as a function of time. The integral buoyancy flux, $q_{int} = \int \langle \mathbf{g} \cdot \mathbf{u}' \frac{\rho'}{\rho} \rangle dr$, has dimensions of velocity cubed. It is convenient to plot kinetic energy and $q_{int}^{3/2}$ on the same graph for detailed comparison. Figure 5 shows the time behavior of damping and driving terms. There are two types of time dependence: (1) a set of bursts (pulses), and (2) a secular increase in amplitude (related to the lack of total balance between nuclear heating and neutrino cooling over the convective zone (Arnett (1996), see Ch. 10).

For a static steady state, these two curves would be almost identical. If for simplicity we assume a planar convective region and neglect the smaller terms in the KE equation (Eq. 1) in favor of buoyancy and damping, we find the simple result $v_{rms}^3/\ell_D \approx \frac{1}{\ell_{CZ}} \int q dr$, or $\ell_D/\ell_{CZ} \approx v_{rms}^3 / \int q dr$.

The power spectra of both curves have a peak at 89 seconds. Both exhibit strong fluctuations; the buoyancy flux precedes the kinetic energy by roughly 20 seconds. *We identify⁵ this lag with the time it takes for the turbulent cascade to react to changes in the flow.* This is suggestively close to our previous estimate of the turbulent decay time of about 14 seconds.

Buoyancy is primarily a property of the largest scales, while damping is a property of the smallest. The large separation of scales means that they are not tightly coupled (except on average), a characteristic of turbulent systems.

The buoyancy flux reaches a high value before turbulence can stop its rise, so that it overshoots the steady state condition. This leads to excessive velocities, which then cascade to excessive damping. In our simulations, the lag in dissipation behind buoyant driving aids fluctuations about the nominal steady state condition.

⁵In implicit large eddy simulations (ILES) like this, the numerical cascade only goes down to the grid scale.

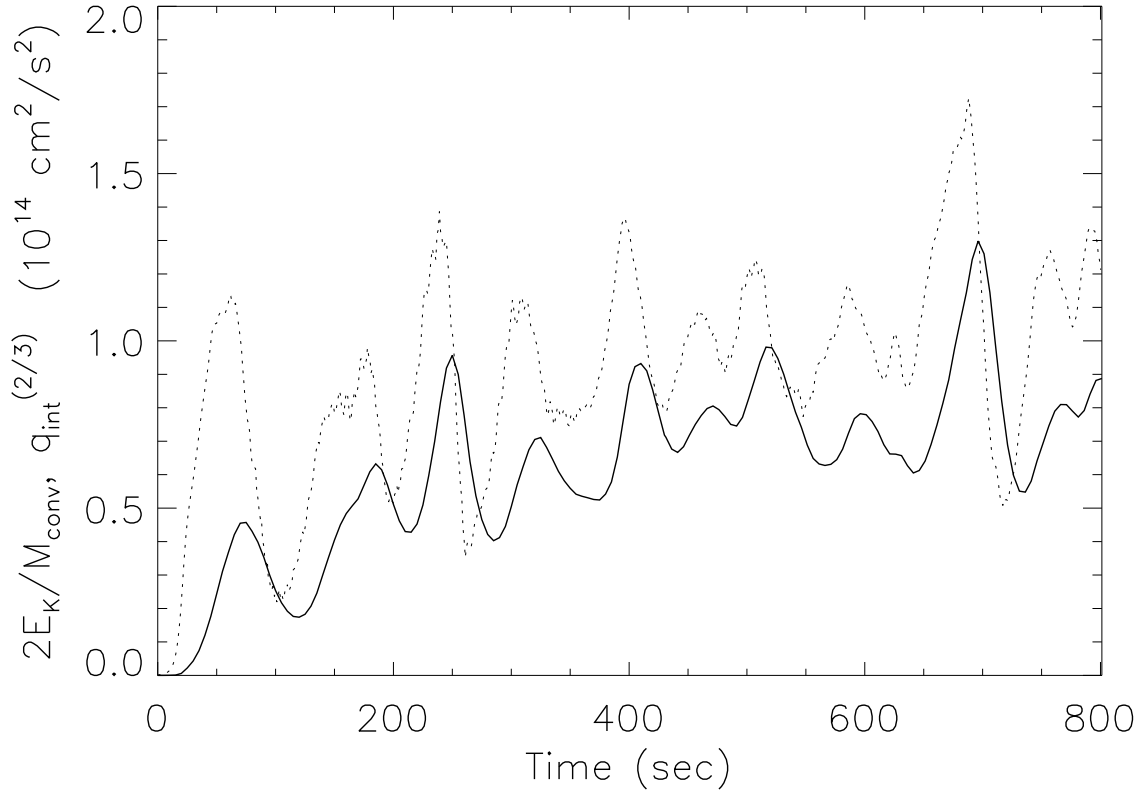


Fig. 5.— Turbulent velocity $v_{rms}^2 = 2E_{turb}/M_{CZ}$ (solid) and $q_{int}^{2/3}$ (dotted) in the convection zone, versus time. Integral buoyancy flux is $q_{int} = \int_{CZ} q dr$, and has units of velocity cubed. Power spectra for both variables peak at 89 seconds; a transit time is 51 s. The kinetic energy lags the buoyant flux by roughly 20 seconds. The average turbulent kinetic energy in the convection zone is about 0.64×10^{47} ergs, with significant fluctuations about that value.

This “boom and bust” cycle is reminiscent of prey-predator relations and the logistic map (May 1976), which also have chaotic behavior. We find that an iterated map of the delay in turbulent damping is quantitatively inadequate to drive the fluctuations. They are driven by nuclear burning, as our simulation (described below) of turbulent decay implies. It will be interesting to explore whether this fluctuating behavior depends upon resolution (we expect it to be dominated by the largest scale eddies, and weakly dependent on resolution).

Consider the average conditions from 200 to 800 seconds in the simulations. The average level of turbulent kinetic energy is about 0.7 of $q_{int}^{2/3}$. If we ignore the smaller terms in the KE equation, we find

$$\alpha_D = \ell_D/\ell_{CZ} = 1.54 u_t^3 / \int q dr \approx 0.89. \quad (16)$$

This is roughly what we get from Table 1, so we conclude that to our accuracy, *the dissipation length in our simulations is roughly the depth of the convective zone*, consistent with Kolmogorov theory. The appearance of ℓ_{CZ} here is due to integration over the convection zone, not to any assumption about the nature of the largest eddies.

2.7. The Decay of Turbulence

The decay of turbulence is a complex topic (Batchelor 1960). Here we will utilize it to provide independent estimates of the damping length. These estimates will differ in detail from those of driven convection because the flow details change, and the dissipation is a function of the flow properties. Nevertheless the sizes of the damping lengths are found to be comparable.

In the left panel in Fig. 6, we show an independent simulation: the rate of decay of turbulent kinetic energy, after oxygen burning and neutrino cooling are artificially turned off at 439 seconds (in the middle of the previous simulation).

If we neglect the small terms for energy flux escaping the convective zone, we may express the kinetic energy equation (Eq. 1) more concisely as $D = dK/dt - B$, where D is the inferred dissipation. After 30 seconds, the buoyancy driving term B becomes small, and dK/dt tracks the turbulent dissipation D . Notice that dK/dt is slightly below D , possibly because of entrainment of stable matter at the convective boundary which requires energy. If we globally fit the inferred damping term by $\varepsilon_K = -M_{CZ} v_{rms}^3/\ell_D$, we have $\ell_D = 4.16 \times 10^8$ cm = 0.97 ℓ_{CZ} .

The right panel in Fig. 6 shows a fit to the kinetic energy, starting 40 seconds after the burning was switched off, and the fossil buoyancy had died away. The kinetic energy may be represented analytically if $dK/dt = D$, so that this late part of the damping curve is reasonably well approximated by a lower damping length, $\ell_D = 2.6 \times 10^8$ cm = 0.61 ℓ_{CZ} .

This independent simulation supports the identification of sub-grid damping with isotropic Kolmogorov damping, and the representation of damping by the global expression (Eq. 5), and $\ell_D \approx (0.6 \text{ to } 1.0)\ell_{CZ}$.

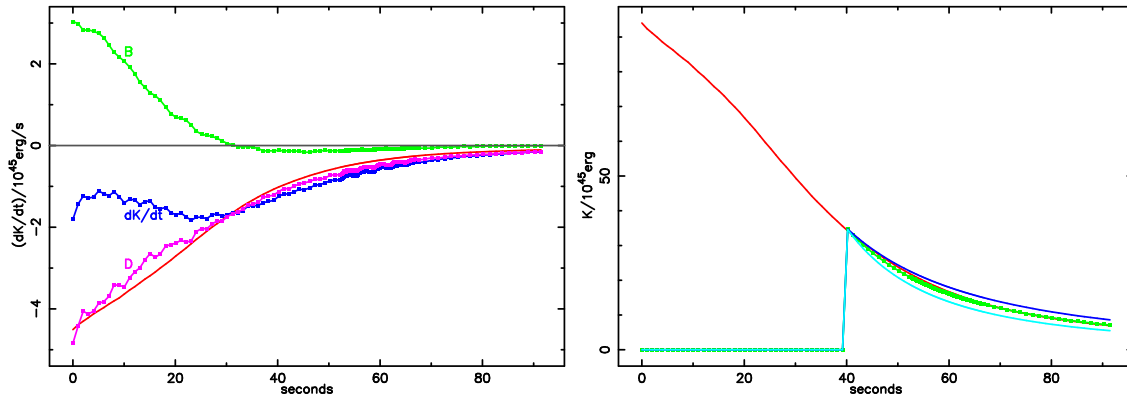


Fig. 6.— (left panel) The rate of decay of turbulent kinetic energy after oxygen burning and neutrino cooling are turned off. The dominant terms are shown: $B = \int W_B d\mathcal{V}$ is the increase of kinetic energy due to buoyant driving, dK/dt is the time derivative of the total kinetic energy in the convection zone, and $D = \int \varepsilon_K d\mathcal{V}$ is the inferred dissipation from the turbulent spectrum ($dK/dt - B$). We assume that little kinetic energy escapes the convection zone. The solid line shows the damping rate approximated by $\varepsilon_K = -M_{CZ} v_{rms}^3 / \ell_D$ with $\ell_D = 4.35 \times 10^8$ cm. After 30 seconds, the buoyancy has died away but damping remains. (right panel) Kinetic energy as a function of time (solid line), and fits of the damping after 40 seconds for $\ell_D/10^8$ cm = 2.1, 2.6 (best) and 3.1. In this phase there is no driving to create anisotropy, and the flow becomes more isotropic on average.

Table 3. Decay Lengths for Different Flows

| Flow | $\alpha_D = \ell_D/\ell_{CZ}$ |
|-----------------------------|-------------------------------|
| Quasi-steady Oxygen Burning | 0.89 |
| Fossil buoyancy in decay | 0.97 |
| Pure decay | 0.61 |

These and the previous estimates for ℓ_D seem to vary beyond the statistical accuracy of the analysis. Replacing the complexity of turbulent dissipation by the simple expression $\varepsilon_K = -M_{CZ} v_{rms}^3 / \ell_D$, with constant ℓ_D is a vast change. This quantity ℓ_D is a property of the flow, and indirectly of the problem being addressed. In particular, the pure decay is more isotropic than the driven cases (Ogilvie 2003). As Table 3 indicates, the ratio ℓ_D / ℓ_{CZ} is different for different flows, but of order unity. Further investigation with different simulations and different physical parameters is needed to understand more precisely the general behavior of ℓ_D .

3. General Equations for Stellar Evolution

How is this approach related to the standard equations of stellar evolution?

3.1. Internal Energy Equation

In MLT a connection is made between superadiabatic gradient $\Delta\nabla$ and convective velocity. This allows the convective enthalpy flux to be expressed in terms of $\Delta\nabla$ (see Kippenhahn & Weigert (1990), § 7, Clayton (1983), § 3-5, and Hansen & Kawaler (1994), § 5). The turbulent kinetic energy equation (Eq. 1) can perform the same function, if the convective velocity is identified with the rms velocity $\langle u'^2 \rangle^{1/2}$ at a given radius, and used in the enthalpy flux in the same way. This replaces the parameterization used in MLT with a physical constraint.

We need to rewrite the total energy equation (A.6 in Meakin & Arnett (2007b)) in the form of the internal energy equation used in stellar evolution. To get the internal energy equation, we subtract the kinetic energy equation (A.12) from the total energy equation (A.6), and find

$$\begin{aligned} \partial_t \langle \rho E_I \rangle + \nabla \cdot \langle \mathbf{u}_0 (\rho E_I + p_0) \rangle = \\ -\nabla \cdot [\mathbf{F}_I + \mathbf{F}_r] - \langle p' \nabla \cdot \mathbf{u}' \rangle \\ + \varepsilon_K + \langle \rho_0 \mathbf{u}_0 \cdot \mathbf{g} \rangle + \langle \bar{\rho} \bar{\epsilon} \rangle. \end{aligned} \quad (17)$$

The left-hand side is just $\rho(dE_I/dt + p_0 dV/dt)$ in lagrangian (co-moving) coordinates (Landau & Lifshitz (1959), see Ch. 1), defining $\rho_0 = 1/V$, so that

$$\begin{aligned} d\langle \bar{E}_I \rangle / dt + \langle \bar{p}_0 dV / dt \rangle = \\ -\frac{1}{\rho_0} \nabla \cdot [\mathbf{F}_e + \mathbf{F}_r] + \langle \bar{\epsilon} \rangle \\ - \langle \frac{p'}{\rho_0} \nabla \cdot \mathbf{u}' \rangle + \varepsilon_K / \rho_0 \\ + \langle \mathbf{u}_0 \cdot (\mathbf{g} - \frac{1}{\rho_0} \nabla p_0) \rangle \end{aligned} \quad (18)$$

The first two lines are the usual terms. Here \mathbf{F}_r is the heat flux due to radiative diffusion, and in this frame the flux of internal energy \mathbf{F}_I becomes the enthalpy flux carried by convection \mathbf{F}_e (see Tennekes & Lumley (1972), p. 33, and our Eq. 12). The nuclear heating term ϵ includes neutrino cooling.

We will rewrite Eq. 18 in more familiar notation (see Arnett (1996), Clayton (1983), Hansen & Kawaler (1994), or Kippenhahn & Weigert (1990)).

$$\begin{aligned}
 dE/dt + PdV/dt = & -\frac{1}{\rho} \nabla \cdot [\mathbf{F}_e + \mathbf{F}_r] + \epsilon \\
 & - \overline{\left\langle \frac{p'}{\rho_0} \nabla \cdot \mathbf{u}' \right\rangle} + \epsilon_K / \rho_0 \\
 & + \overline{\left\langle \mathbf{u}_0 \cdot \left(\mathbf{g} - \frac{1}{\rho_0} \nabla p_0 \right) \right\rangle}
 \end{aligned} \tag{19}$$

The first line contains the usual formulation. The new terms are: $\overline{\left\langle \frac{p'}{\rho_0} \nabla \cdot \mathbf{u}' \right\rangle}$ which represents the compressional work done by pressure fluctuations (which also appears in the kinetic energy equation and we have seen to be small here), ϵ_K / ρ_0 which is the deposition of heat by the Kolmogorov turbulent cascade, and $\overline{\left\langle \mathbf{u}_0 \cdot \left(\mathbf{g} - \frac{1}{\rho_0} \nabla p_0 \right) \right\rangle}$, which is zero in hydrostatic equilibrium without rotation or expansion, and drives meridional circulation for rotating, radiative stars (Tassoul 1978; Clayton 1983).

The ϵ_K / ρ_0 term allows turbulent kinetic energy to do dissipative heating, a new effect not in conventional stellar evolution, and it is not guaranteed to be negligible. Through Eq. 1 it couples the divergence of the kinetic energy flux (including rotational shear) and the wave energy flux to the internal energy. As an internal energy source term, it can generate entropy and cause mixing even in radiative regions. For the Sun, this term would give rise to heating in the photosphere, chromosphere and corona by shocks and wave motion (pressure and Alfvén waves), for example.

Equations 1 and 19 represent an extension of turbulent convection theory for stellar evolution, in which (1) the algebraic relation for convective velocity and superadiabatic gradient is replaced by a differential equation (see Spiegel (1972)), and (2) the Kolmogorov cascade is explicit in the formulation. Notice that both space and time derivatives appear, making the system nonlocal and time dependent, unlike MLT. These derivatives allow the treatment of boundary dynamics in a physical way. We will explore specific implementations in a subsequent paper, including entrainment at convective boundaries.

Let us now consider some simplifications in order to clarify the meaning of these equations. In particular, we assume time invariance (so the time derivatives are small on average), no overall background motion ($\mathbf{u}_0 = 0$), and little work done by pressure perturbations on the velocity perturbations. As shown previously, these are reasonable approximations except in extreme cases. Then Eq. 1 becomes

$$\overline{\left\langle \rho' \mathbf{g} \cdot \mathbf{u}' \right\rangle} - \nabla \cdot (\mathbf{F}_K + \mathbf{F}_P) = \epsilon_K, \tag{20}$$

and Eq. 19 becomes

$$\rho\epsilon - \nabla \cdot (\mathbf{F}_e + \mathbf{F}_r) = -\epsilon_K \quad (21)$$

The coupling of internal energy and turbulent kinetic energy occurs through the Kolmogorov cascade, which creates internal energy by damping kinetic energy. Eliminating ϵ_K , we have

$$\rho\epsilon = -\overline{\langle \rho' \mathbf{g} \cdot \mathbf{u}' \rangle} + \nabla \cdot (\mathbf{F}_e + \mathbf{F}_P + \mathbf{F}_r + \mathbf{F}_K). \quad (22)$$

In a steady state, the nuclear energy generation must balance the divergence of fluxes out of the region and supply the work needed to maintain the convective flow. This is different from the usual formulation used in stellar evolution in that there are new terms ($-\overline{\langle \rho' \mathbf{g} \cdot \mathbf{u}' \rangle} + \nabla \cdot (\mathbf{F}_K + \mathbf{F}_P)$), which combine to equal ϵ_K , the dissipation rate due to the Kolmogorov turbulent cascade. If the turbulent velocity is nonzero, these corrections are also nonzero, leading to the conclusion that the standard formulation of stellar evolution is wrong in neglecting turbulent heating. The motion implied by convection will carry kinetic energy, drive pressure and gravity waves into radiative regions, and give local microscopic heating as it dissipates in a transit time, effects that should no longer be ignored in stellar evolution. Through its dependence on ζ , for a given convective enthalpy flux, the kinetic energy flux is dependent upon the equation of state.

For a low Mach-number flow and radial coordinates,

$$\overline{\langle \rho' \mathbf{g} \cdot \mathbf{u}' \rangle} = \beta_T g F_e / C_P T, \quad (23)$$

so that $\nabla \cdot \mathbf{F} \rightarrow dL/dm$, then Eq. 22 becomes

$$\epsilon = -\frac{\nabla_a}{m_p} L_e + \frac{d}{dm} (L_e + L_P + L_r + L_K), \quad (24)$$

where $\nabla_a = \beta_T P V / C_P T$, $m_p = 4\pi r^2 \rho H_P$, and H_P is the pressure scale height. For an ideal gas, $\nabla_a \rightarrow (\gamma - 1)/\gamma$, or 0.4 for $\gamma = 5/3$. For gases with a specific heat at constant pressure which is large compared to the specific heat at constant volume (such as partially ionized plasma or electron-positron plasma), ∇_a is smaller (see below).

4. Comparison to Other Simulations

Table 4. A Comparison of Parameters from some 3D simulations

| Reference | ℓ_{CZ}/H_P | α_T | α_E | α_v | EOS | Bnd. | Zones |
|--------------------------|-----------------|------------|------------|-------------------|----------------|------|--------|
| Meakin & Arnett (2007b) | 2.0 | 0.73 | 0.70 | 1.22 | <i>e</i> -pair | yes | 4.0(6) |
| Porter & Woodward (2000) | 4.5 | 2.04 | 0.80 | 2.70 | ideal | grid | 6.7(7) |
| Chan & Sofia (1989) | 4.8 | 1.05 | 0.83 | 2.16 | ideal | grid | 3.6(4) |
| Kim et al. (1995) | 6.0 | 1.42 | 0.85 | 2.16 | ionize | yes | 3.3(4) |
| Chan & Sofia (1996) | 6.8 | 1.30 | 0.68 | 2.60 | ideal | yes | 4.8(5) |
| MLT | | $\alpha/2$ | 1.0 | $\alpha/\sqrt{2}$ | | | |

These theoretical ideas may be tested by application to other simulations of turbulence. Several groups have compared 3D simulations to MLT predictions (Chan & Sofia 1989, 1996; Kim et al. 1995, 1996; Meakin & Arnett 2007b; Porter & Woodward 2000; Porter, Woodward, & Jacobs 2000), and published sufficient detail to allow easy quantitative comparison. All agree that MLT is somewhat successful, but derive different values for some of the MLT parameters. This suggests that these parameters may not be universal, but a function of the conditions of the simulated flow, and that our theoretical analysis may be able to put them on a common basis. See also Abbett, et al. (1997); Ludwig et al. (1999); Trampedach, et al. (1999); Brandenburg, et al. (2005), who have also compared simulations to MLT.

These simulations are not a homogeneous set, so that global comparisons on this data set must be taken with caution. Porter & Woodward (2000) and Meakin & Arnett (2007b) used PPM codes while the Yale group (Chan & Sofia 1989, 1996; Kim et al. 1995; Robinson et al. 2004) used compressible viscous codes with sub-grid scale modelling (and much lower resolution). Chan & Sofia (1996) and Meakin & Arnett (2007b) had the convection zone bounded by stable regions while the others did not; these boundary conditions give rise to new phenomena (Meakin & Arnett 2006, 2007a). The deeper convection zones developed more anisotropic flows, and velocities approaching the sound speed (e.g., Cattaneo, et al. (1991); Woodward, Porter, & Jacobs (2003)). Porter & Woodward (2000) carefully attempted to compensate for these effects, the Yale group used damping to tame them, and the soft equation of state and shallower depth made them small for Meakin & Arnett (2007b) (see below). Porter & Woodward (2000) found that they needed to shift the apparent mixing length by about 30 percent, down from $\alpha = 3.53$ to $\alpha = 2.68$. The simulations of Meakin & Arnett (2007a) included an oxygen-burning shell (with an electron-positron equation of state, see Table 5), and those of Kim et al. (1995) and Robinson et al. (2004) included a solar photosphere (with strong ionization effects in the equation of state). Our simulations are driven by nuclear heating at the bottom of the convection zone; the others are driven by cooling at the upper boundary (like the Sun).

Table 4 summarizes the inferred parameters. The entries are ordered in increasing depth of the convective zone as measured in pressure scale height units (ℓ_{CZ}/H_P), which corresponds to increasing asymmetry in the vertical direction. The choice of equation of state (ideal gas, e^-e^+ -pair gas, ionized plasma) and of the boundary conditions affect the simulations. Even the definition of the depth of the convective zone may be modified depending on whether the grid includes the stable bounding region ("yes") or not ("grid"). The bottom line in the table gives the traditional MLT values for several parameters (Kippenhahn & Weigert 1990). The last column gives the number of zones on the computational grid.

4.1. Convection Parameters

We now examine each of a set of important convection parameters (see Porter & Woodward (2000) and Meakin & Arnett (2007b) for details). These parameters reflect the various uses of the MLT parameter α , and are a convenient and concise way to compare the simulations of compressible turbulent convection.

4.1.1. α_T

In 3D simulations, a correlation is found between rms temperature fluctuation $(T')_{rms} = \langle T'^2 \rangle^{\frac{1}{2}}$ and the superadiabatic gradient $\Delta\nabla = \nabla - \nabla_a - \nabla_x$, using the conventional notation in astrophysics of $\nabla = \partial \ln T / \partial \ln P$ (Kippenhahn & Weigert 1990; Hansen & Kawaler 1994; Clayton 1983). Here, $\nabla_a = \partial \ln T / \partial \ln P$, taken at constant entropy and composition, and $\nabla_x = -\nabla_\mu$ is the remaining part due to possible compositional change. Then,

$$(T')_{rms}/T_0 = \alpha_T \Delta\nabla, \quad (25)$$

on average, over time and over the volume of the convection zone. Consider low Mach-number flow so that $\rho'/\rho_0 = -\beta_T (T'/T_0)$.

In a single convective roll (e.g., Lorenz (1963); Tritton (1988)), T' is the temperature perturbation amplitude at the horizontal mid-plane. In the vertical mid-plane of the roll, $T' = [(dT/dr) - (dT/dr)_{ad}] \ell_{CZ}/2$ is the corresponding amplitude. Assuming the amplitudes are comparable,

$$T'/T_0 = (\ell_{CZ}/2H_P) \Delta\nabla, \quad (26)$$

implying that $\alpha_T \approx \ell_{CZ}/2H_P$, and not a constant. In MLT, $\alpha_T = \alpha/2$, which is a particular choice for the assumed flow.

In the simple picture of a single convective roll, $(T')_{rms}/T_0$ can give a buoyancy torque, while $\Delta\nabla$ cannot, because the gravitational acceleration vector is directed radially downward (Tritton 1988). In the Lorenz (1963) model of thermal convection, the difference between the two is intimately connected to the onset of chaotic behavior. Meakin & Arnett (2007b) find $\alpha_T \approx 0.73$ (see their Fig. 17), so that

$$\alpha_T = 0.73 \ell_{CZ}/2H_P. \quad (27)$$

There is considerable variation in the values of α_T shown in Table 4, with a tendency to increase for deeper (more stratified) convection zones.

Notice that for two convective rolls, one atop the other, we would expect the characteristic roll size to change ($\ell \approx \ell_{CZ} \rightarrow \ell_{CZ}/2$, so $\alpha_T \rightarrow \alpha_T/2$, approximately). This explicitly shows how the convection parameters can be a function of the properties of the flow itself.

Figure 7, left panel, shows the behavior of α_T as a function of the depth of the convection zone, for the computations listed in Table 4. The two PPM calculations (Meakin & Arnett (2007b)

and Porter & Woodward (2000)) agree with the scaling indicated in Eq. 27. The calculations using the compressible viscous equations with sub-grid modelling for dissipation all lie below Eq. 27. In order to give some idea of the depth needed in simulations of stellar convection zones, the x -axis in Fig. 7 is marked from zero to the depth of the solar convection zone (20 pressure scale heights). None of these simulations describe such an extremely anisotropic case.

4.1.2. α_E and α_K

The enthalpy flux is

$$\begin{aligned} F_c &= \rho_0 C_P \overline{T' u'} \\ &= \alpha_E \rho_0 C_P (T')_{rms} (u')_{rms}, \end{aligned} \quad (28)$$

where Meakin & Arnett (2007b) find $\alpha_E = 0.70 \pm 0.03$; in Table 4, α_E is relatively constant among the simulations (the total range is about 20 percent). It is not ruled out that α_E might be a universal constant, or at least slowly varying. Note that α_E is just the correlation coefficient for T' and u' . It seems that α_E is not sensitive to the Prandtl number Pr . Porter & Woodward (2000) have a different Pr (ours is $Pr \approx 1$) and get an α_E similar to ours.

Using Eq. 25, this becomes

$$F_c = \alpha_E \alpha_T \rho_0 C_P T_0 (u')_{rms} \Delta \nabla. \quad (29)$$

Similarly, if the kinetic energy flux is

$$F_K = \frac{1}{2} \langle \rho u'^2 u'_z \rangle, \quad (30)$$

we may define

$$\alpha_K = \langle \rho u'^2 u'_z \rangle / \langle \rho \rangle \langle (u'_z)^2 \rangle^{3/2}, \quad (31)$$

so that $F_K = \frac{\alpha_K}{2} \langle \rho \rangle \langle (u'_z)^2 \rangle^{3/2}$. Note that the sign of α_K can be negative.

4.1.3. α_v

In Meakin & Arnett (2007b), the correlation between convective velocity (squared) and super-adiabatic excess $\Delta \nabla$ is written as

$$(u')_{rms}^2 = (\alpha_v^2 / 4) g \beta_T H_P \Delta \nabla. \quad (32)$$

In MLT, a similar expression is defined, with $\alpha^2/8$ replacing $\alpha_v^2/4$. If we have local balance between buoyancy driving and turbulent damping,

$$\langle \rho' g u' \rangle \approx \langle \rho \rangle (u')_{rms}^3 / \ell_D. \quad (33)$$

using Eq. 13, Eq. 25, and Eq. 28, we have

$$(u')_{rms}^2 = (\ell_D \alpha_T \alpha_E) \beta_T g \Delta \nabla. \quad (34)$$

Comparing this to Eq. 32 we have

$$\alpha_v^2/4 = \alpha_T \alpha_E \ell_D / H_P. \quad (35)$$

Using Eq. 27 and $\alpha_E = 0.70$,

$$\alpha_v = 1.22 (\ell_{CZ}/2H_P)(\ell_D/0.9\ell_{CZ})^{\frac{1}{2}} \quad (36)$$

In Table 4 we see that α_v is variable, and tends to increase with increasing depth of the convective zone. This is shown explicitly in the right panel of Fig. 7. The two PPM calculations are in excellent agreement with Eq. 36, taking $\ell_D = 0.9 \ell_{CZ}$ ($\alpha_D = 0.9$), while the three compressible viscous calculations lie below it.

Using Eq. 29, we have

$$F_c = (\alpha_E \alpha_T \alpha_v / 2) \rho_0 C_P T_0 \sqrt{g \beta_T H_P} (\Delta \nabla)^{3/2}. \quad (37)$$

Using Eq. 27, Eq. 36, $\ell_D = 0.9\ell_{CZ}$ and $\alpha_E = 0.70$, we have

$$\alpha_E \alpha_T \alpha_v / 2 = 0.312 (\ell_{CZ}/H_P)^2, \quad (38)$$

for the factor in Eq. 37.

4.2. The electron-positron Plasma

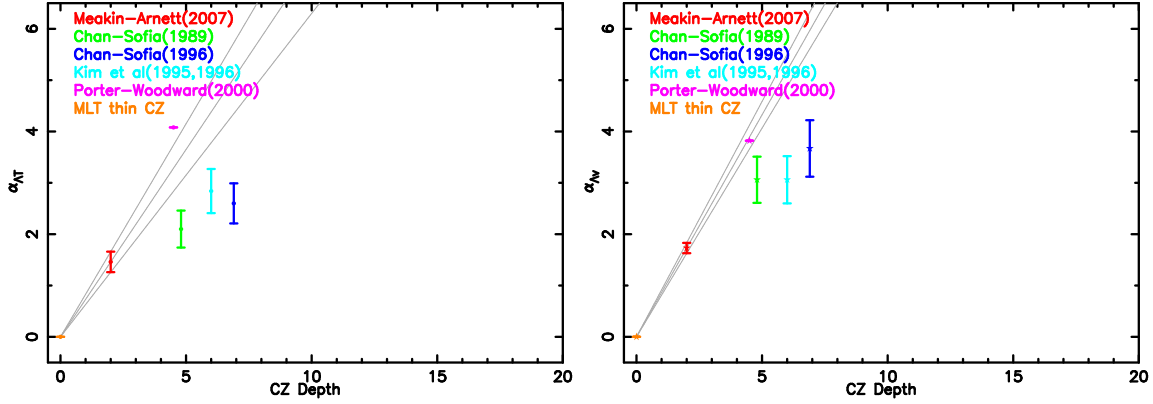


Fig. 7.— Predicted $2\alpha_T = \alpha_{\Lambda,T}$ (top panel) and $\sqrt{2}\alpha_v = \alpha_{\Lambda,v}$ (bottom panel), as a function of depth of the convective zone in units of H_P . This scaling (Meakin & Arnett 2007b) gives “alphas” which are comparable to the MLT values and each other. Some of the error bars are large; new simulations are needed to determine how well such results follow a single curve (Meakin & Arnett, in preparation). In the limit of small depth, the mixing length must be no larger than the depth itself; hence the point at zero depth is an analytic result. The Meakin & Arnett (2007b) and Porter & Woodward (2000) points and the origin are close to colinear. It appears that both α_T and α_v are functions of depth of the convective region, and not universal constants.

Table 5. Thermodynamic parameters for Entropy $S/\mathcal{R} = 4.623$

| T_9 | ρ_6 | $\ln P_{max}/P$ | C_P/\mathcal{R} | β_T | $PV/C_P T$ | ∇_{ad} |
|-------|----------|-----------------|-------------------|-----------|------------|---------------|
| 2.51 | 1.580 | 0.0 | 15.36 | 3.912 | 0.0609 | 0.2382 |
| 2.31 | 1.225 | 0.348 | 14.53 | 3.757 | 0.0638 | 0.2397 |
| 2.11 | 0.930 | 0.724 | 13.62 | 3.592 | 0.0673 | 0.2417 |
| 1.91 | 0.690 | 1.134 | 12.67 | 3.421 | 0.0714 | 0.2443 |
| 1.71 | 0.498 | 1.583 | 11.73 | 3.257 | 0.0762 | 0.2483 |
| 1.51 | 0.348 | 2.080 | 10.83 | 3.106 | 0.0814 | 0.2529 |

The thermodynamic character of the electron-positron plasma in the oxygen burning shell is significantly different from an ideal gas, an effect which must be taken into account in comparisons to simulations which use different equations of state. This is illustrated in Table 5; we use the Helmholtz equation of state of Timmes & Swesty (2000). The entropy in the oxygen burning convection zone is $S/\mathcal{R} \approx 4.6$ in dimensionless units, where \mathcal{R} is the gas constant. The zone is about 2 pressure scale heights deep (see column 3). For an ideal gas, the specific heat at constant pressure is $2.5\mathcal{R}$; C_P/\mathcal{R} is much larger for the plasma, ranging between 10 and 16 (column 4). Column 5 gives the value of β_T , which is unity for an ideal gas, but lies between 3 and 4 for the plasma. Column 6 gives the ratio of $PV/C_P T = p_0/\rho_0 C_P T_0$, which is 0.4 for an ideal gas. The ratio of the buoyancy flux to the enthalpy flux (Eq. 14) is proportional to $\nabla_a = \beta_T PV/C_P T$. The same factor appears in the ratio of the kinetic energy flux to the enthalpy flux. For the ideal gas $\nabla_a = 0.4$, but is smaller for the plasma (column 7). For the same convective enthalpy flux, the pair-plasma has a lower kinetic energy flux, so the velocity scale is lower.

4.3. Direction of the Kinetic Energy Flux

The kinetic energy flux is averaged over angle at a given radius, and averaged over two convective turnover times. As Fig. 5 shows, this time span covers significant dynamic behavior. Roughly speaking, an unstable configuration forms, becomes dynamic, reforms, becomes dynamic again, and so on. Over this turnover timescale the nuclear burning provides the energy necessary to drive the turbulent kinetic energy ($\epsilon\tau \approx \frac{1}{2}\overline{u'^2}$).

The convective instability is closely related to the Rayleigh-Taylor instability (Chandrasekhar, S. 1961), which has been produced dramatically in high energy-density plasma experiments (Remington et al. 1999), i.e., under star-like conditions and well into the nonlinear growth regime. The characteristic behavior is the rise of mushroom-shaped higher entropy plasma and the fall of spike-shaped lower entropy plasma. If we consider a closed volume, these motions are accompanied by slower return motions which maintain mass conservation. The kinetic energy flux scales with velocity cubed, and so is dominated by the fast moving mushrooms and spikes. In a symmetrical system we will have an upward kinetic energy flux (from the mushrooms) in the region above the horizontal midplane of the volume, and a downward kinetic energy flux in the region below. If we average over several cycles (turnover times) the kinetic energy flux will be dominated by these motions, being positive (upward) above the midplane and negative below. This is qualitatively similar to the simulation results of Meakin & Arnett (2007b) (see their Fig. 21 and Fig. 22).

This simple picture is complicated by an up-down asymmetry due to stratification (hydrostatic structure). The depth of the convection zone in pressure scale heights, $\ell_{CZ}/H_P = \ln(P_{bot}/P_{top})$, is a direct measure of the up-down asymmetry. Upward flows move into regions of lower pressure, and expand; downward flows move into regions of higher pressure, and are compressed. The smaller area of the downflows implies higher velocities relative to a coordinate frame containing

the convection zone (a lagrangian frame). This will favor downward (negative) kinetic energy fluxes. The neglect of kinetic energy fluxes (Böhm-Vitense 1992) corresponds to the limiting case of a shallow convection zone. For deep convection zones, there is a strong bias in favor of fast downward plumes (Nordlund & Stein 2000; Stein & Nordlund 1998), and these dominate the flow for simulations with $\ell_{CZ}/H_P \geq 4$ or so. In Meakin & Arnett (2007b), which has a depth $\ell_{CZ}/H_P = 2$, the convective zone is skewed, so that the surface, which separates the positive and the negative kinetic energy fluxes, moves nearer to the bottom of the convection zone. For Porter & Woodward (2000), where ℓ_{CZ}/H_P is larger, the positive kinetic energy flux is overwhelmed, and the direction of the kinetic energy flux is opposite to that of the much larger enthalpy flux. We expect this to be a general property of deep convection zones.

There is a natural limit to the depth of convection zones expected in active burning regions. Entropies in active burning regions vary relatively slowly (Arnett (1996), Ch. 10), so that the depth of a convection zone implies a value of the temperature ratio between bottom and top. In Table 5, the convection zone extends down almost to neon burning temperatures ($T \approx 1.5 \times 10^9$ K). Further extension will entrain new fuel into the oxygen convective shell, which will burn at the *top* of the convection zone, choking the flow. For the last stages (C, Ne, O and Si burning), the burning temperatures for different fuels are fairly close together, implying that their related convection zones will tend to be relatively shallow. They are also close together in radius, raising the issue of interactions between them (Meakin & Arnett 2006).

Here $\ell_{CZ}/H_P = \ln P_{bot}/P_{top} = \frac{\gamma}{\gamma-1} \ln T_{bot}/T_{top}$. For example, for advanced burning stages or radiation dominated regions, $\gamma \approx 4/3$, and $\gamma/(\gamma-1) = 4$. For helium and hydrogen burning, $T(He)/T(H) \approx 13$ so $\ell_{CZ}/H_P \leq 4 \ln 13 \approx 10$. A helium burning convective zone will not be deeper than about 10 scale heights unless the overlying matter is devoid of hydrogen. For carbon burning the corresponding depth is $\ell_{CZ}/H_P \lesssim 3$, unless devoid of H and He fuel. Surface convection zones may extend down to the hydrogen burning regions. Very roughly, $\ln T(H)/T_e \approx 8$, so $\ell_{CZ}/H_P \lesssim 32$, using the structure of an $n = 3$ polytrope.

4.4. Magnitude of the Kinetic Energy Flux

Table 6. Comparison of some 3D simulations

| Reference | ℓ_{CZ}/H_P | ∇_a | F_K/F_c |
|--------------------------|-----------------|------------|------------------|
| Meakin & Arnett (2007a) | 2 | 0.24 | -0.018 +0.014 |
| Porter & Woodward (2000) | 4.5 | 0.40 | -0.3 |
| Cattaneo, et al. (1991) | 5 | 0.40 | -0.35 |
| Chan & Sofia (1989) | 4.8 | 0.40 | -0.35 |
| Chan & Sofia (1996) | 6.8 | 0.40 | -0.50 |

Table 6 gives the ratio of kinetic energy flux to enthalpy flux for several 3D simulations. This ratio is much smaller in our simulations (by a factor of 35 to 50) than in the others, and F_K changes sign in our convection zone.

As in (Meakin & Arnett 2007b) we can write the KE to enthalpy flux ratio according to mixing length relationships,

$$\frac{F_K}{F_c} \sim \frac{\rho v_c^2 / 2}{\rho c_p T'} \frac{v_c}{v_c} \sim \left(\frac{\alpha_v^2}{8\alpha_T} \right) \nabla_a \quad (39)$$

and then balance between buoyancy driving and turbulent damping through Eq. 35 gives

$$\frac{F_K}{F_c} \sim \frac{\alpha_D \alpha_E}{2} \left(\frac{l_{CZ}}{H_P} \right) \nabla_a. \quad (40)$$

See Eq. 3.14 of Porter & Woodward (2000), which uses a gamma-law equation of state to generate the sum of kinetic and enthalpy fluxes, and implies an equivalent flux ratio.

The ratio of ∇_a for the ideal gas to that of the electron-positron gas gives a factor of 1.6 or so. The ratios of the depth of the convection zones give another factor of ~ 5 . While these considerations illustrate the role played by the depth of the convection zone and go some way towards explaining the trends in KE flux it is also important to consider the geometry of the driving region, which relates to how well a local balance between buoyancy driving and turbulent damping is achieved as assumed in Eq. 35. In particular, the length scale l_a over which buoyancy is imparted to the stellar plasma through either heating at the base of the convection zone or cooling at the top can affect the KE to enthalpy flux ratio dramatically. This may be understood simply: the flow depends both upon the geometry of the convective domain and upon the way in which the fluid is stirred. At present we have at least two basic patterns, a mostly negative kinetic energy flux for deep convective zones driven by surface cooling (most stellar surface convection zones) and a more complex positive-negative convective flux for shallower zones driven by nuclear burning. More simulations are underway to clarify this issue (Meakin and Arnett, in prep.).

4.5. Saturation of Kinetic Energy Flux

Are there limits to the linear rise in energy of convection that is implied by Fig. 7? Deep convection zones ($l_{CZ} \geq 4H_P$) have strong negative kinetic energy fluxes. For very deep zones, the extrapolated kinetic fluxes imply supersonic velocities. Such large velocities would generate shock waves, which would increase dissipation, converting kinetic energy into internal energy. The rate scales as the velocity difference cubed, which is the same scaling as turbulent dissipation in the Kolmogorov cascade (Bethe 1942; Boris 2007). This suggests that even if deeper convection zones did tend to have increasingly strong velocities, shock dissipation will become significant, and

resist the increase of ℓ_D with increasing ℓ_{CZ} . In this sense, the increase in damping length must “saturate” with increasing depths.

Increased damping may come sooner from another effect: a change in the nature of the eddies and the size of the damping length. Physically this would occur as follows: as the deep, fast, narrow downflows drive into the convection zone they will give rise to shear instabilities at their interfaces, which will lead to mixing with the ambient fluid, and exchange momentum through a turbulent viscosity, and eventually completely dissolve into the background. This would give shorter dissipation lengths, and would begin to occur before the mach numbers become large enough for significant shock formation.

We expect the PPM calculations for deeper convective zones to “flatten” in Figure 7 as the Yale simulations do, but at higher amplitude, due to increased damping with increased depth. This hypothesis needs to be tested numerically, which will be challenging. Shock waves may cause errors at grid boundaries, deep convection zones will have longer thermal relaxation times, and maintaining sufficiently wide aspect angle implies many computational zones for adequate resolution, for example.

The simulations of the Yale group (Chan & Sofia 1989, 1996; Kim et al. 1995, 1996; Robinson et al. 2004), which use fewer zones and a strong damping (Smagorinsky 1963), appear to have a larger dissipation than the PPM simulations (Porter & Woodward 2000; Meakin & Arnett 2007b). This is qualitatively equivalent to the saturation discussed above, and may be tested if calculations using the Yale code (or equivalent) are repeated at higher resolution and/or lower dissipation.

5. Some Implications

5.1. Waves

The energy flux terms include both advective transport and waves. Here we will recall some properties of waves and their generation (Landau & Lifshitz (1959), Press (1981)). The characteristic frequencies of convective motion are centered about a frequency $\omega_{CZ} \approx v_{rms}/\ell_{CZ}$. The convective mach number, $(u')_{rms}/\mathcal{C} = \rho'/\rho_0 = p'/\rho_0\mathcal{C}^2$, is a measure of compressibility of the flow; here \mathcal{C} is the sound speed. If the interface between convective and radiative zones moves with the matter (is volume conserving, on average), it generates acoustic waves by dipole emission at a luminosity $L_{p-mode} \propto \omega_{CZ}^6$ (see Landau & Lifshitz (1959), § 73), or as the Mach number to the sixth power. For more vigorous motion, the perturbation may give volume changes, so that the acoustic wave generation by monopole emissivity, or Mach number to the fourth power. For subsonic flows this channel is closed to significant energy flow, but open as $(u')_{rms}$ approaches the local sound speed, as it does in the surface convection zones of many stars, including the Sun, or as it may in the stage prior to core collapse in massive stars.

While the exact power dependence may depend upon specific geometries and degree of interfer-

ence, a general result seems to be: the gravity wave channel dominates over the acoustic channel for low mach number flows (as we observe in our simulations, see Meakin & Arnett (2007a) for a more detailed discussion of both the g-mode and p-mode behavior, including mixed p- and g- modes). Both types of waves are generated by convection interacting with stably stratified bounding regions, and the luminosity of each depends upon both the convective vigor and the impedance at the boundary. Such waves can propagate into stably stratified regions (Press 1981; Press & Rybicki 1981; Young & Arnett 2005). Generation of gravity waves by convective turbulence has become an issue in questions of mixing and angular momentum transport (García López & Spruit 1991; Charbonnel & Talon 1999; Talon & Charbonnel 2004; Young & Arnett 2005).

The establishment of a robust estimate of the turbulent velocity field should improve estimates of wave generation, which has implications for mass loss, mixing in radiative regions, coronal heating and helioseismology. In particular, the pressure correlation flux takes over the energy carried by the kinetic energy flux as the convective boundaries are approached. This gives a direct connection between the scale of turbulent velocity and g-mode wave emission (Press 1981).

5.2. Rotation and Magnetic Fields

A closely similar set of mean-field equations are used in the theory of the magnetic resonance instability (MRI) in accretion disks (Balbus & Hawley 1998; Pessah, Chan, & Psaltis 2006). If we had included magnetic fields in the MHD approximation, and assumed strong rotation, our procedure would have produced an equation for mechanical energy (our Eq. 1 corresponds to Eq. 17 of Balbus & Hawley (1998)), and total energy (Eq. A6 of Meakin & Arnett (2007b) to their Eq. 27). Projection onto a cylindrical coordinate system, with the rotational axis oriented parallel to the total angular momentum vector, would give an angular momentum equation (their Eq. 29.). Auxiliary equations provide for magnetic field dynamics, radiation transport, and nuclear burning. This underlying similarity provides a way to write a more general set of mean-field equations, of which both stars and accretion disks are limiting cases. In turn this allows a systematic evaluation of the relative importance of different effects (rotational mixing and convective mixing, for example) which are now considered piecemeal.

Our simulations include the complete set of rotational terms, but the initial conditions imply that these terms are not exercised except as convectively induced shear. Our simulations do not include magnetic fields in the MHD approximation, but could be generalized to do so (Stone & Gardiner 2007; Pessah, Chan, & Psaltis 2006). Because they interact, rotation and magnetic fields should be included together.

Balbus & Hawley (1994) have argued that in the stellar case, the weak-field MRI dominates over merely hydrodynamic instabilities, and drives the radiative zones (but not convective zones) toward solid body rotation. Heger, Langer, & Woosley (2000) argued the reverse (based on the Høiland instability criterion), that convective zones would tend toward rigid body rotation, and

radiative zones would tend to have differential rotation. Because the Høiland instability applies to neutral fluids, not dense plasma, it is probably not relevant for stars. Helioseismology (Thompson, et al. 1996; Howe, et al. 2005; Brandenburg 2007) is showing that while the convective zone of the Sun shows differential rotation, the underlying radiative zone seems to be tending toward solid body rotation, as the MRI arguments suggest. (Browning & Basi 2007) have shown that even deep convection zones can generate significant magnetic fields, so that the presence of a stable interface is not necessary for field generation. The rotational state of the central regions of the Sun probably depends upon the efficacy of angular momentum transport by processes related to flow of the plasma, including g-mode waves (Charbonnel & Talon 1999), as well as magnetic fields.

5.3. Damköhler Number for Burning

In general, it is appropriate to decompose the equations in temperature ($T = T_0 + T'$) and composition as well. The opacity and the nuclear reaction rates are often sensitive to both. Meakin & Arnett (2006) found flashing due to oxygen burning in vigorous downdrafts which were fuel-rich (the flashes were too mild to affect the flow dramatically). None of these effects are included in standard stellar evolution theory. For simplicity we suppress this complication for the moment; this means that our opacities and reaction rates are to be interpreted as averages over fluctuations in these variables as well. Further investigation of this issue, with 3D simulations, is desirable.

For this set of simulations, the heating and cooling times are at least 100 times longer than the transit times, so that we are in the regime of small Damköhler number $D_m \lesssim 0.01$ (Zel'dovich, Barenblatt, Librovich, & Makhviladze 1985; Oran & Boris 1987). The release of nuclear energy during a transit time is small relative to the internal energy in the convection zone, but comparable to the superadiabatic energy and to the turbulent kinetic energy. The burning drives the turbulent motions, but only gives moderate pulses of kinetic energy, as shown in Fig. 5. This is unlike the much more complex problem of Type Ia supernova models, for which D_m is large. In our case the necessary averaging over convective cycles does not seem to be a problem.

This convenient state may not apply to the double shell flash stage for asymptotic giant branch stars, in which wave driven mixing and entrainment are likely to complicate the issue of mixing, and therefore figure into the question of s-process nucleosynthesis (Busso et al. 1999; Campbell & Lattanzio 2008).

6. Summary

We find that our three-dimensional time-dependent simulations of compressible stellar turbulence (ILES) are well represented by a master equation (Eq. 1) for kinetic energy which includes

dissipation implied by the Kolmogorov cascade. The damping length is found in three independent ways, with reasonable consistency, and is the size of the largest eddy, which is approximately the geometric linear dimension (depth) of the convective zone. Unlike the mixing length of MLT, it is not a free parameter, but a mathematical consequence of the turbulent flow. Balancing turbulent buoyant driving with Kolmogorov damping provides a reasonable estimate of the damping length. The divergence of kinetic energy and acoustic fluxes is nonzero, and provides the mechanism to spread turbulence through the convective zone, and make the Kolmogorov damping a good approximation. The turbulent flow is highly dissipative and must be maintained by continual driving; this “frictional heating” term is missing from the standard stellar evolution equations, as are the kinetic energy and acoustic fluxes.

Fluctuations in kinetic energy are significant (of order 50 percent), and damping lags driving by about a transit time for the convective zone.

Comparison with some other simulations, which were dramatically different in many respects, gives a consistent picture. Turbulent convection is more vigorous for deeper (more stratified) convection zones. Turbulent kinetic energies are lower for nonideal equations of state, such as partially ionized plasmas and electron-positron plasmas, to the extent that their specific heat at constant volume is less than their specific heat at constant pressure. The average flow structure changes in a simple way depending upon the depth of the convection zone; deep convection zones have downwardly directed flows of kinetic energy, cancelling some of the upward enthalpy flux.

It appears that extension of this approach, using simulations to define stellar convection algorithms, can establish a theoretical model of turbulent convection that does not require astronomical calibration, but can be based upon a combination of computer simulations, terrestrial observations, and experiments. Efforts to implement this general theory in a stellar evolution code are underway.

During the course of this project, we lost two friends who were leaders in the field of stellar evolution, John Bahcall and Bohdan Paczynski, to whom this paper is dedicated. This work was supported in part by NSF Grant 0708871 and NASA Grant NNX08AH19G at the University of Arizona, and the ASCII FLASH center at the University of Chicago. One of us (DA) wishes to thank the Aspen Center for Physics and the International Center for Relativistic Astrophysics (ICRA) for their hospitality, Brian Chaboyer for help with the history of the mixing length implementation, Martin Pessah for discussions of MRI physics, Robert Stein for discussion of the effect of the continuity equation on flows, Vittorio Canuto for helpful discussions of the philosophy of turbulence modelling, Martin Asplund for providing machine-readable copies of solar surface models, and Frank Timmes for helpful comments on the draft and for providing access to the Saguaro computer cluster. We wish to thank an anonymous referee for insightful comments which improved both our presentation and our understanding.

A. Decomposition

We decompose velocity, density, and pressure fields into mean and fluctuating components according to

$$\varphi = \varphi_0 + \varphi', \quad (\text{A1})$$

where $\overline{\langle \varphi \rangle} = \varphi_0$ and $\overline{\langle \varphi' \rangle} = 0$ and the overbar and brackets indicate time and horizontal averaging, respectively. For data handling and analysis purposes we consider the fluctuating component of the field to be composed of a radial p-mode component and a component due to all other sources

$$\varphi' = \varphi'_p + \varphi'_t. \quad (\text{A2})$$

This additional decomposition allows us to make a more accurate estimate of the fluctuations associated with turbulent convection in the presence of a coherent radial p-mode which is not well sampled in the output files from the simulation. If the radial p-mode contribution were well sampled then we would find $\overline{\langle \varphi'_p \rangle} = 0$ to the degree that the mode is adiabatic.

Consider the radial velocity to be composed of the following components

$$u = u_0 + u'_p + u'_t, \quad (\text{A3})$$

where u_0 is the mean background expansion, u'_p is the radial p-mode induced fluctuation, and u'_t is the fluctuation due to turbulent convection and other non-radial modal components. Averaging, we find

$$\overline{\langle u \rangle} = \overline{\langle u'_p \rangle} + \overline{\langle u'_t \rangle} + u_0. \quad (\text{A4})$$

Because of our poor sampling of the low order radial p-modes which have frequencies comparable to the simulation data output rate ($\delta t \approx 0.5$ s) we find that the term $\overline{\langle u'_p \rangle} > 0$ and contributes a significant error to the estimation of u'_t . In order to correct for this horizontally coherent p-mode induced radial displacement, we subtract the horizontally averaged radial velocity component at each time step and estimate the turbulence induced fluctuation by

$$u'_t = u - \langle u'_p \rangle - u_0 \approx u - \langle u'_p \rangle. \quad (\text{A5})$$

The latter approximate equality in the above equation is made because of the smallness of the background expansion compared to the the r.m.s. velocity fluctuations associated with the turbulent convection, $u_0/u'_c \sim 10^{-3}$.

The instantaneous fluctuations in pressure and density are calculated according to

$$p'_t = p - \langle p \rangle, \tag{A6}$$

and,

$$\rho'_t = \rho - \langle \rho \rangle. \tag{A7}$$

REFERENCES

- Abbett, W. P., et al. , 1997, ApJ, 480, 395
- Arnett, D., 1996, *Supernovae and Nucleosynthesis*, Princeton University Press, Princeton NJ
- Asida, S.M., & Arnett, D. 2000 ApJ, 545, 435
- Balbus, S. A., & Hawley, J. F., 1994, MNRAS, 266, 769
- Balbus, S. A., & Hawley, J. F., 1998, Rev. Mod. Phys., 70, 1
- Batchelor, G. K., 1960, *Homogeneous Turbulence*, Cambridge University Press
- Bethe, H. A., 1998, in *Classic Papers in Shock Compression Science*, Springer-Verlag, New York, (Original report NDRC-B-237, 1942)
- Biermann, L., 1951, ZAp, 28, 305
- Boris, J., 2007, in *Implicit Large Eddy Simulations*, ed. F. F. Grinstein, L. G. Margolin, & W. J. Rider, Cambridge University Press, p. 9
- Böhm-Vitense, E., 1958, ZAp, 46, 108
- Böhm-Vitense, E., 1992, *Introduction to Stellar Astrophysics*, Vol. 3 *Stellar Structure and Evolution*, Cambridge University Press, Cambridge
- Brandenburg, Axel, Chan, K. L., Nordlund, A., & Stein, R. F., 2005, *Astronomische Nachrichten*, 326, 681
- Brandenburg, Axel, in *Handbook of the Solar-Terrestrial Environment*, eds. Y. Kamide & A. C.-L. Chian, Springer, in press, and astro-ph/0703711
- Browning, M., 2008, ApJ, 676, 1262
- Browning, M. K., & Basri, G., 2007, astro-ph:0711.3474v1.
- Busso, M., Gallino, R., & Wasserburg, G. J. 1999, ARA&A, 37, 239
- Campbell, S. W., & Lattanzio, J. C., 2008, *First Stars III*, 990, 315

- Cattaneo, F., Brummel, N., Toomre, J., Malagoli, A., Hurlburt, N. E., 1991, ApJ, 370, 282
- Chandrasekhar, S. 1961, *Hydrodynamic and Hydromagnetic Instability*, Oxford University Press, London
- Chan, K. L., & Sofia, S. 1989, ApJ, 336, 1002
- Chan, K. L., & Sofia, S. 1996, ApJ, 466, 372
- Chandrasekhar, S., 1961, *Hydrodynamic and Hydromagnetic Stability*, Oxford University Press, Oxford, GB
- Charbonnel, C., & Talon, S., 1999, A&A, 351, 635
- Clayton, D. D. 1983, *Principles of Stellar Evolution and Nucleosynthesis*, University of Chicago Press, Chicago
- Cvitanović, P., 1989, *Universality in Chaos*, Adam Hilger, Bristol and New York
- Dutton, J. A., 1986, *The Ceaseless Wind*, Dover Publications, Inc., Mineola, NY
- Fernando, H. J. s. 1991, Annual Review of Fluid Mechanics, 23, 455
- Frisch, U., 1995, *Turbulence*, Cambridge University Press, Cambridge
- García López, R. J. & Spruit, H. C. 1991, ApJ, 377, 268
- Gill, A. E., 1982, *Atmospheric-Ocean Dynamics*, Academic Press, San Diego CA
- Gleick, J., 1987, *Chaos: Making a New Science*, Penguin Books, New York
- Hansen, C. J., & Kawaler, S. D., 1994, *Stellar Interiors*, Springer-Verlag
- Heger, A., Langer, N., & Woosley, S. E., 2000, ApJ, 528, 368
- Howe, R., et al. , 2005, ApJ, 634, 1405
- Kim, Y.-C., Fox, P. A., Demarque, P., & Sofia, S., 1996, ApJ, 461, 499
- Kim, Y.-C., Fox, P. A., Sofia, S., & Demarque, P., 1995, ApJ, 442, 422
- Kippenhahn, R. & Weigert, A. 1990, *Stellar Structure and Evolution*, Springer-Verlag
- Kolmogorov, A. N., 1941, Dokl. Akad. Nauk SSSR, 30, 299
- Kolmogorov, A. N., 1962, J. Fluid Mech., 13, 82
- Kritsuk, A. G., Norman, M. L., Padoan, P., & Wagner, R., 2007, ApJ, 665, 416
- Landau, L. D. & Lifshitz, E. M., 1959, *Fluid Mechanics*, Pergamon Press, London

- Lorenz, E. N., 1963, *Journal of Atmospheric Sciences*, 20, 130
- Ludwig, H.-G., Freytag, B., & Steffan, M., 1999, *A&A*, 346, 111
- May, Robert M., 1976, *Nature*, 261, 459
- Meakin, C., & Arnett, D., 2006, *ApJ*, 637, 53
- Meakin, C., & Arnett, D., 2007a, *ApJ*, 665, 690.
- Meakin, C., & Arnett, D., 2007b, *ApJ*, 667, 448.
- Meynet, G., & Maeder, A., 2000, *A&A*, 361, 101
- Nordlund, A., & Stein, R., 2000, *The Impact of Large-Scale Surveys on Pulsating Star Research*, ASP Conf. Series, 203, 362
- Obukhov, A. M., 1962, *J. Fluid Mech.*, 13, 77
- Ogilvie, G. I., 2003, *MNRAS*, 340, 969
- Oran, E. S., & Boris, J. P., 1987, *Numerical Simulation of Reactive Flow*, Elsevier Science Publ. Co., New York
- Pessah, M. E., Chan, C-K., & Psaltis, D., 2006, *Phys. Rev. Lett.*, 97, 221103
- Porter, D. H., Pouquet, A., Sytine, I., & Woodward, P. R., 1999, *Physica A*, 263, 263
- Porter, D. H., & Woodward, P. R., 2000, *ApJS*, 127, 159
- Porter, D. H., Woodward, P. R., & Jacobs, M. L., 2000, *Ann. N. Y. Acad. Sci.*, 898, 1 (Proceedings of Fourteenth International Annual Florida Workshop in Nonlinear Astronomy and Physics, *Astrophysical Turbulence and Convection*, University of Florida, Feb. 1999).
- Press, W. H. 1981, *ApJ*, 245, 286
- Press, W. H. & Rybicki, G. 1981, *ApJ*, 248, 751
- Remington, B. A., Arnett, D., Drake, R. P., Takabe, H. 1999. Modeling Astrophysical Phenomena in the Laboratory with Intense Lasers. *Science* 284, 1488.
- Robinson, F. J., Demarque, P., Li, L. H., Sofia, S., Kim, Y.-C., Chan, K. L., & Guenther, D. B. 2004, *MNRAS*, 347, 1208
- Schüssler, M., & Völger, A., 2008, *A&A*, 484, L17
- Shannon, C., 1948, *Bell System Technical Journal*, 27, 379
- E.E.,

- Spiegel, E. 1972, *ARA&A*, 10, 261
- Smagorinsky, J., 1963, *Mon. Weather Rev.*, 91(3), 99
- Stein, R. F., and Nordlund, Å., 1998, *ApJ*, 499, 914
- Stone, J., and Gardiner, T., 2007, *ApJ*, 671, 1696
- Sytine, I., Porter, D., Woodward, P., Hodson, S. W., & Winkler, K-H., 2000, *J. Chem. Phys.*, 118, 225
- Talon, S., & Charbonel, C., 2004, *A&A*,
- Tassoul, J.-L. 1978, *Theory of Rotating Stars*, Princeton University Press, Princeton NJ
- Tennekes, H., & Lumley, J. L., 1972, *A First Course in Turbulence*, MIT Press, Cambridge MA
- Thompson, J. M. T. & Stewart, H. B., 1986, *Nonlinear Dynamics and Chaos*, John Wiley and Sons, New York
- Thompson, M. J., et al. , 1996, *Science*, 272, 1300
- Timmes, F. X. & Swesty, F. D. 2000, *ApJS*, 126, 501
- Trampedach, R., Stein, R. F., Christensen-Dalsgaard, J., & Nordlund, A., 1999, in *Stellar Structure: Theory and Tests of Convective Energy Transport*, ASP Conference Series, 173, ed. E. F. Guinan and B. Montesinos, Astronomical Society of the Pacific, San Francisco, p 233.
- Tritton, D. J., *Physical Fluid Dynamics*, 2nd ed., Oxford University Press, Oxford UK
- Turner, J. S., 1973, *Buoyancy Effects in Fluids*, Cambridge University Press, Cambridge UK
- Vitense, E., 1953, *ZAp*, 32, 135
- Woodward, P., 2007, in *Implicit Large Eddy Simulations*, ed. F. F. Grinstein, L. G. Margolin, & W. J. Rider, Cambridge University Press, p. 130
- Woodward, P. R., Porter, D. H., & Jacobs, M., 2000, in *3D Stellar Evolution*, ed. S. Turcotte, S. C. Keller, & R. M. Cavallo, ASP Conference Series 293, p. 45
- Young, P. A. & Arnett, D. 2005, *ApJ*, 618, 908
- Zel'dovich, Ya. B., Barenblatt, G. I., Librovich, V. B., & Makhviladze, G. M., 1985, *Combustion and Explosions*, Plenum Publishing Corporation, New York